Timing of sea level, tectonics and climate events during the uppermost Oxfordian (Planula Zone) on the Iberian ramp (northeast Spain)

Colombié, C.[1], Giraud, F.[2], Schnyder, J.[3], Götz, A.E.[4], Boussaha, M.[5], Aurell, M.[6], Bádenas, B.[6]

[1] *Laboratoire de Géologie de Lyon, Université Claude Bernard Lyon 1, La Doua, bâtiment Géode, 69622 Villeurbanne cedex, France (claude.colombie@univ-lyon1.fr)*
[2] *ISTerre, Université de Grenoble 1, UMR 5275, 1381 rue de la piscine, F- 38041 Grenoble, France*
[3] *UMR 7193 ISTeP, Université Pierre et Marie Curie-Paris 6, case 117, 4 place Jussieu, 75252 Paris cedex 05, France*
[4] *University of Pretoria, Department of Geology, Private Bag X20, Hatfield, 0028 Pretoria, South Africa*
[5] *University of Copenhagen, Department of Geosciences and Natural Resource Management, Øster Voldgade 10, Copenhagen 1350, Denmark*
[6] *Dpto. Ciencias de la Tierra, Universidad de Zaragoza, 50009-Zaragoza, Spain*

ABSTRACT

The middle Oxfordian warming climate and sea-level rise initiated the development of vast carbonate platforms in some western European basins. At the same time, however, siliciclastics and siliceous sponges dominated certain marginal areas of the Iberian ramp. There, siliciclastic input was particularly prominent during the latest Oxfordian and may have been related to a global sea-level fall, synsedimentary tectonic activity, or humid climatic conditions in the hinterland. Field analyses and computer modeling have been previously used to determine the factors that controlled sedimentation. However, it is still unclear if the specific conditions that prevailed during the latest Oxfordian were due to eustasy, tectonics or climate, and when precisely they occurred. Here, we document major changes in sedimentological, micropalaeontological, and mineralogical records on the Iberian ramp during this interval. Detailed sedimentary facies and palynofacies analyses combined with sequence-stratigraphic and cyclostratigraphic analyses of the Ricla Barranco section enable the establishment of a high-resolution time frame. Based on the quartz and mica percentage fluctuations, one large- and seven small-scale sequences are defined. The large-scale sequence boundaries correlate with third-order sequence boundaries Ox8 and Kim1 defined by Hardenbol et al. (1998). The large-scale maximum-flooding surface corresponds to the base of the most calcareous interval and to the maximum abundance of marine phytoplankton and opaque, equidimensional phytoclasts. The small-scale sequences correspond to the 100-kyr orbital eccentricity cycle. Calcareous nannofossils and clay minerals were used as palaeoclimatic proxies. Nannofossil abundances and fluxes are lower in the upper part than in the lower part of the interval studied, suggesting a decrease in sea-surface trophic conditions, also shown by an increase in the relative abundance of oligotrophic taxa. This upper part is also characterised by an increase in smectite, which coincides with the base of the large-scale highstand deposit, and is interpreted as reflecting the establishment of dry conditions. A first increase in smectite occurs in the lower part of the succession, and coincides with high percentages of quartz and mica. This latter mineralogical assemblage is interpreted as recording the onset of the Late Jurassic to Early Cretaceous rifting stage, which occurred just before the Planula–Galar ammonite Subzone transition. The present study points out a return toward optimum conditions for carbonate sedimentation only 300 kyr after the prominent increase in siliciclastic input due to tectonic activity. The recovery of carbonate production was accompanied by a global sea-level rise and by decreasing rainfall on nearby land.

1. Introduction

The middle Oxfordian warming and rise in sea level favoured the development of broad carbonate platforms in some western European basins (e.g., Aurell et al., 2010; Brigaud et al., 2014; Dromart et al., 2003; Pellenard et al., 2014). At the same time, certain marginal areas of the Iberian ramp presented a very different kind of sedimentation in which siliciclastics and siliceous sponges dominated. In particular, the influence of siliciclastics was prominent during the latest Oxfordian, which has been related to tectonic activity (Bádenas and Aurell, 2001; Aurell et al., 2010). During the Late Jurassic and the Early Cretaceous, the evolution of the Iberian rift system is linked to northward propagation of rifting from the central Atlantic and the gradual opening of the North Atlantic oceanic basin (Martin-Chivelet et al., 2002). The Iberian basin, located in the central eastern part of the plate is one of these rift systems (Alvaro et al., 1978; Salas and Casas, 1993; Van Wees et al, 1998). The intracontinental rifting started in this basin during the latest Oxfordian. The reactivation of some basement faults at the end of the Oxfordian induced both the uplift of the edges and the subsidence of the middle part of the ramp (e.g., Aurell and Meléndez, 1993). When compared to the middle Oxfordian, the late Oxfordian coral reefs in the northern hemisphere developed in a more southward position (Martin-Garin et al., 2012). These reefs contain abundant microbialites, which reflect meso- to eutrophic conditions and suggest nutrient input under a humid climate. Eutrophication due to high terrigenous input or local palaeoceanographic changes producing cold-water influxes would explain the absence of coral reefs on the Iberian ramp during the Oxfordian (Aurell et al., 2010). Field analyses and computer modeling have been previously used to better understand the factors that controlled sedimentation (Aurell et al., 1995; 1998). However, it is still unclear if these specific conditions were eustatically, tectonically or climatically induced, and when exactly they occurred. So far, high-frequency cycles, probably eustatic and climatic in origin, have been defined in the interval comprising the base of the Transversarium ammonite Zone and the top of the Bimammatum Zone (Strasser et al., 2005).

Here, we document major changes in sedimentological, micropalaeontological, and mineralogical records on the Iberian ramp during this key period of the late Oxfordian. The Ricla Barranco section has been chosen because its stratigraphic record is complete due to its location on the subsiding mid-ramp. Detailed facies and palynofacies analyses combined with high-resolution sequence-stratigraphic and cyclostratigraphical interpretations enable the stratigraphic correlation with contemporaneous series in adjacent basins and the definition of a high-resolution time frame. As suitable material for oxygen-isotope measurements to determine palaeotemperature was lacking, calcareous nannofossils and clay minerals were used as palaeoclimatic proxies. Calcareous nannofossil assemblages are affected by variations in trophic and thermal regime of sea surface waters and their fluctuations in abundance can be partly interpreted as climatic changes. Clay minerals resulting from the alteration of primary minerals reflect specific climatic conditions. The present study is the first attempt to reconstruct sea level, tectonic, and climatic events within the latest Oxfordian with a time-resolution in the order of 100 kyr.

2. Geological setting

In the Iberian basin of northeast Spain, during the Late Jurassic, shallow and
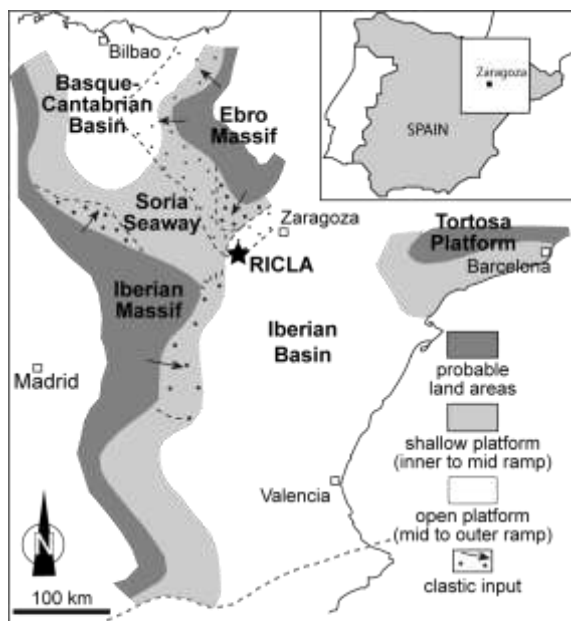
Fig. 1. Palaeogeography of the Middle-Late Oxfordian in NE Spain (modified from Aurell et al., 2003; Bádenas and Aurell, 2001; Strasser et al., 2005).

homoclinal ramps opened toward the East, into the Tethys Sea (Fig. 1). Tectonic events around the Oxfordian–Kimmeridgian boundary caused significant changes in the sedimentation pattern, which led to a major unconformity between the Oxfordian and the Kimmeridgian depositional sequences (i.e., depositonal sequences J3.1 and J3.2 in Aurell and Meléndez, 1993 see Fig. 2). According to the available ammonite biostratigraphy (e.g., Bádenas et al., 1998; Delvene, 2001; Strasser et al., 2005), the studied succession at Ricla Barranco corresponds to the entire Planula Zone of the Tethyan province, which includes the Planula and the Galar subzones (Fig. 2). The boundary between these two subzones is located close to bed 145 in the section studied (Delvene, 2001) (Fig. 3). The Planula Zone, traditionally assigned to the Upper Oxfordian, is considered to be coeval with the lowermost Kimmeridgian of the Boreal province (Matyja et al., 2006 in Gradstein et al., 2012) (Fig. 2).

The interval studied comprises the siliciclastic-rich "middle interval" and the marly-dominated "upper interval" of the Sot de Chera Formation (Bádenas et al., 1998) (Fig. 2). These two lithological units are bounded by a regional unconformity located at the boundary between the Planula and the Galar subzones.

The coarsening-up siliciclastic-rich "middle interval" of the Sot de Chera Formation resulted from the more proximal deltaic system progradation as part of the highstand systems tract of the Oxfordian depositional sequence J3.1 (Aurell and Meléndez, 1993) (Fig. 2). The thickness of this interval has significant lateral variability, suggesting synsedimentary tectonic activity. The tectonic reactivation of some basement faults by the end of the Oxfordian also involved the uplift of the edges of the basin and the increase of the coarse clastic sediment supply (e.g., Aurell et al., 2010).

The "upper interval" of the Sot de Chera Formation mostly comprises marls with a high amount of mica and plant remains, and scattered ostracodes, bivalves and scarce ammonites, pointing to a low-energy, relatively open-marine environment (Aurell et al., 1998; 2010). These marls display a wedge-shaped geometry, and were interpreted as belonging to the lowstand systems tract of the Kimmeridgian depositional sequence J3.2 (Aurell and Meléndez, 1993) (Fig. 2), or as having been deposited during the early transgressive stage of
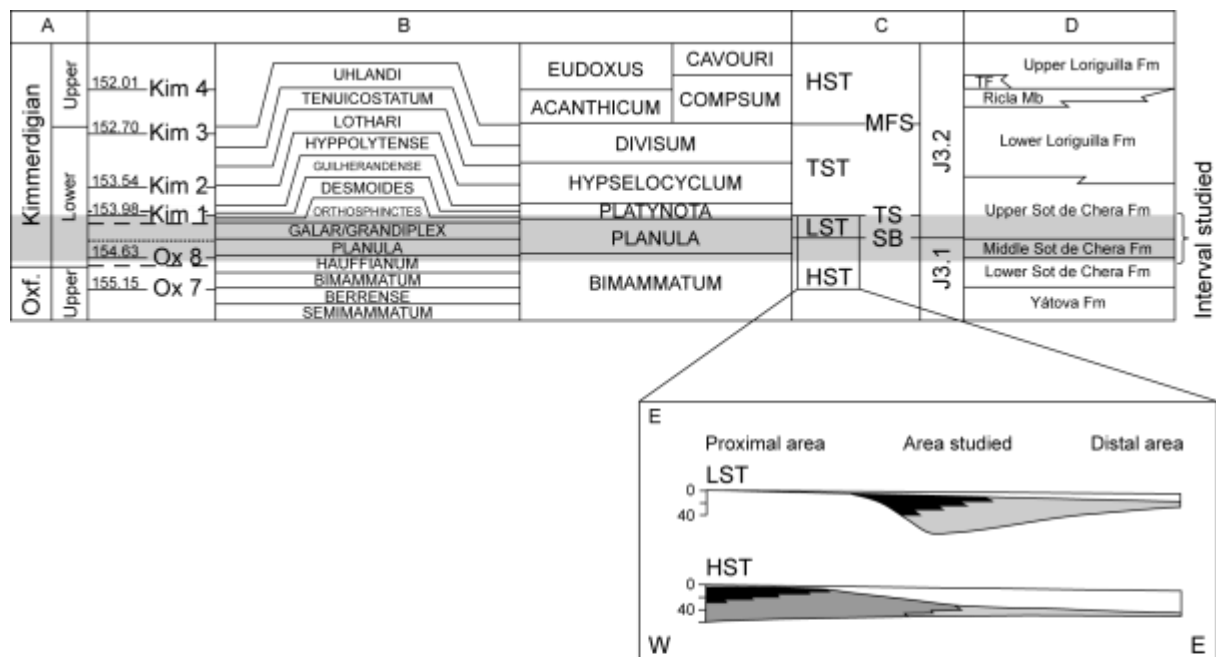
Fig. 2. Chronostratigraphic location and evolution of the interval studied. A) Stages (Gradstein et al., 2012); B) Third-order sequence boundaries (SB: full line; TS: dotted line; MFS: dashed line) and Tethyan ammonite subzones and zones (Hardenbol et al., 1998); C) NE Spain systems tracts, stratigraphic surfaces, and sequences (Aurell and Meléndez, 1993); D) NE Spain lithostratigraphic units (TF: Torecilla Fm) (Bádenas et al., 1998; Bádenas and Aurell, 2001); E) Cross-sections showing the sedimentary evolution of the interval studied in NE Spain (Aurell and Meléndez, 1993).

the T-R Kimmeridgian sequence (e.g., Aurell et al., 2003; 2010).

While eustatic fluctuations probably controlled sedimentation during the early and the middle Oxfordian, the late Oxfordian deposits mainly recorded the local synsedimentary tectonics (Aurell and Meléndez, 1993). Aurell et al. (1995) used computer modeling to address the relative importance of the various factors that are considered to control the origin and the evolution of the Iberian Late Jurassic carbonate ramps. They showed that the geometries observed in the field come from the superposition of 20 and 100 kyr cycles on a third-order cycle. The higher-order cycles are in the Milankovich frequency band and may be eustatic in origin. The third-order cycle and its timing do not correspond to the Exxon eustatic curve and may be a local, relative sea-level change.

3. Materials and methods

The Ricla Barranco section, called Ri8 in Aurell (1990) and Delvene (2001), or 1 in Bádenas et al. (1998), is located 6 km north-northwest of the village of Ricla in the Zaragoza province of northeastern Spain (Fig. 1). The exposed succession is 103 metres thick and spans the entire Upper Oxfordian Planula Zone. The section was studied with respect to sedimentary and organic facies, sequence- and cyclostratigraphy, calcareous nannofossils, and clay mineralogy.
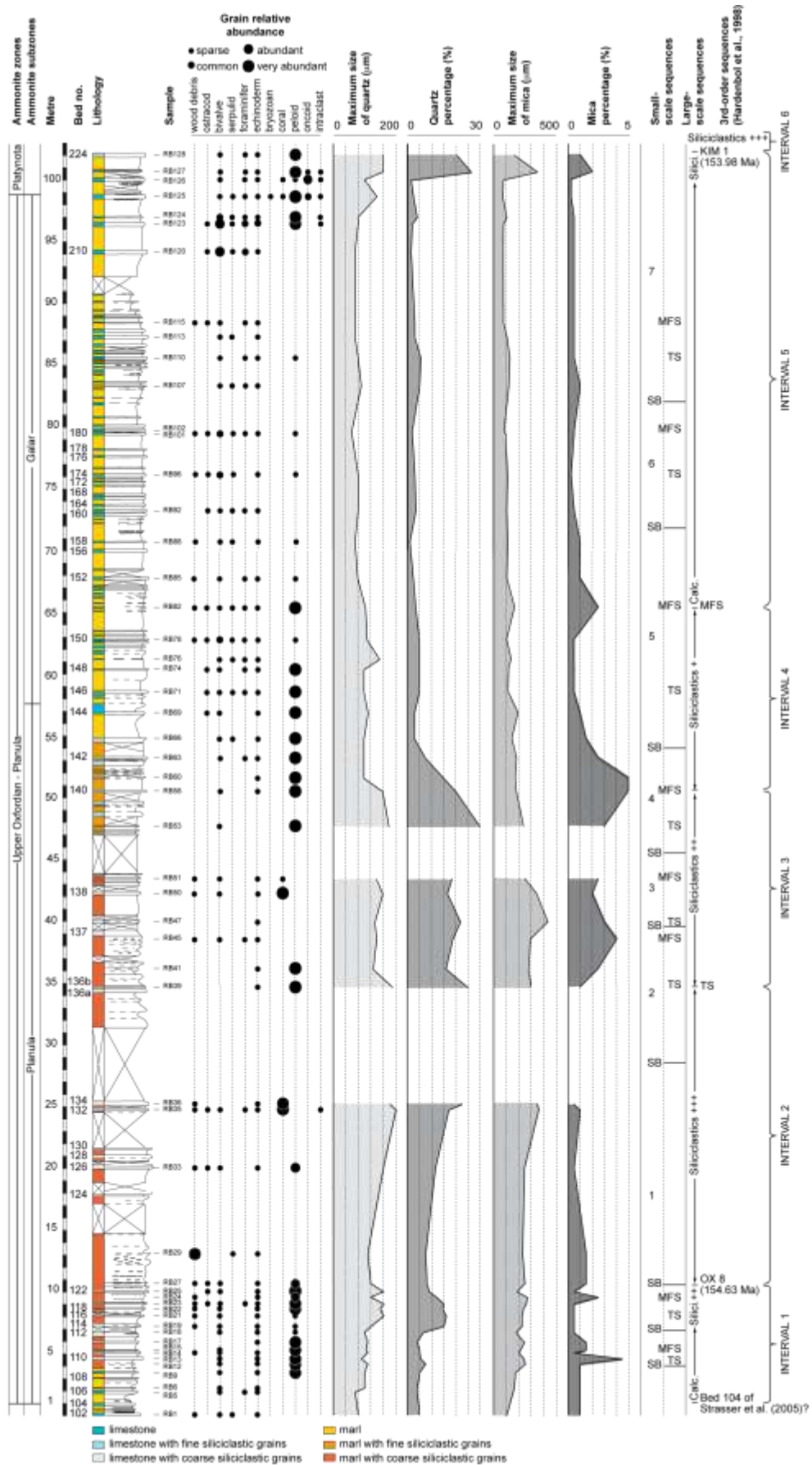
Fig. 3. Facies and microfacies analyses and sequence-stratigraphical interpretation of the Ricla Barranco section.

## 3.1. Sedimentary facies, sequence- and cyclostratigraphy

The methodology and nomenclature summarized in Catuneanu et al. (2011) is applied to define the sequence stratigraphic framework. This framework relies on field and thin section observations. The Ricla Barranco section was logged bed by bed. Figure 3 includes the measured outcrop section, thicknesses in metres, bed numbers according to Delvene (2001), and lithology. A total of 55 samples and thin sections were analysed. The relative abundance of grains and the maximum size and the percentage of quartz and mica were determined in thin sections. The relative abundance of grains ranges between sparse and very abundant (Fig. 3). Grains are sparse when their number is higher or equal to one in a thin section; common when their number is higher or equal to one in each field of view of the microscope at a magnification of × 40; abundant when their number is higher or equal to two in each field of view, and very abundant when their number is strictly higher than two in each field of view, the fields of view covering the entire thin section. The maximum size of quartz and mica is the average of the 10 largest grains (Pettijohn et al., 1987). The percentages of quartz and mica were estimated by comparison with the Baccelle and Bosellini (1965) charts. These data were used to determine the depositional environments. For the sequence-stratigraphic interpretation, deepening-up and shallowing-up facies trends, which may correlate with transgression and regression, respectively (Catuneanu et al., 2011), define stratal stacking patterns that are interpreted as deposits. The term "deposit" is used instead of systems tracts because the geometry of the sedimentary bodies is not visible in one section alone (Strasser et al., 1999). Deposits have different types of bounding stratigraphic surface at the top and at the base (Catuneanu et al., 2011). Lowstand deposits (LSDs) include deposits that accumulate between the end of the relative sea-level fall, which coincides with the sequence boundary (SB), and the end of regression, corresponding to the transgressive surface (TS). Transgressive deposits (TDs) comprise the deposits that accumulate between the TS and the maximum of transgression, which is the maximum-flooding surface (MFS). Highstand deposits (HSDs) develop between the MFS and the next SB. Regressive deposits include HSDs and LSDs, while transgressive deposits form TDs. Criteria used for the recognition of these deposits have to be defined, as they depend on the particularities of the case study (Catuneanu et al., 2011). Deposits and stratigraphic surfaces form sequences, which correspond to relative sea-level cycles (Catuneanu et al., 2009 in Catuneanu et al., 2011). The high-resolution sequence-stratigraphic interpretation and cyclostratigraphical analysis follow the concepts of Strasser et al. (1999). The stacking pattern of sequences commonly reveals a hierarchical pattern. The smallest recognisable cycles of relative sea-level change are called elementary sequences. They stack into small-scale sequences, which in turn form medium and large-scale sequences. The criteria used for the recognition of these hierarchically stacked sequences are independent of scale (Colombié and Strasser, 2005). This nomenclature is purely descriptive and does not imply duration as long as the time framework is not known. This time framework is defined according to stratigraphic correlation with the Hardenbol et al. (1998) and Gradstein et al. (2012) chronostratigraphic charts by means of the ammonite biostratigraphy confirmed by Delvene (2001) in the Ricla Barranco section. The cyclostratigraphical interpretation relies on the number of sequences in a given time span and their hierarchical organisation.

3.2. Palynofacies

A total of 46 samples of the uppermost Oxfordian Planula Zone were studied with respect to their sedimentary organic matter content (Fig. 4). All samples were prepared using standard palynological processing techniques, including HCl (33 %) and HF (73 %) treatment
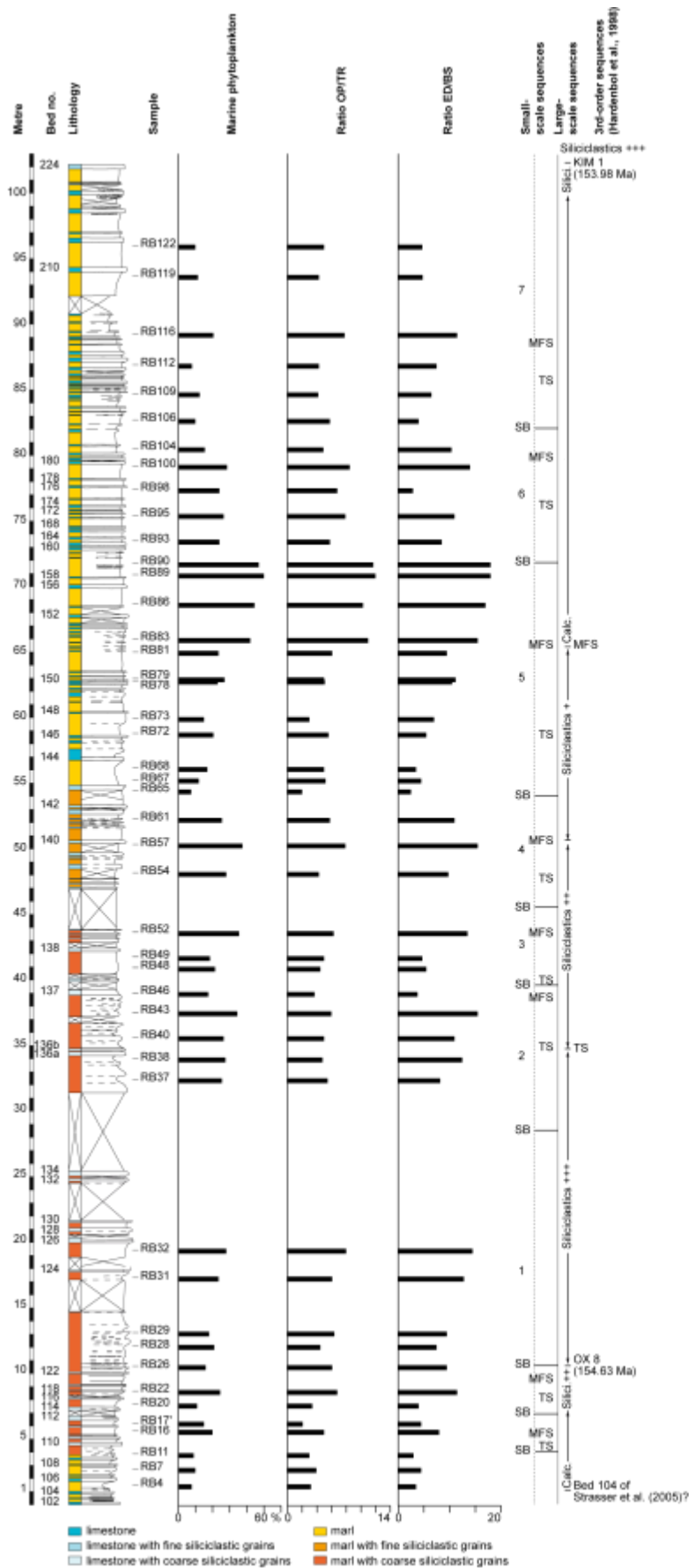
Fig. 4. Palynofacies of the Ricla Barranco section. Maximum flooding is documented by maximum abundance of marine phytoplankton and opaque, equidimensional phytoclasts (interval 65-72 m).
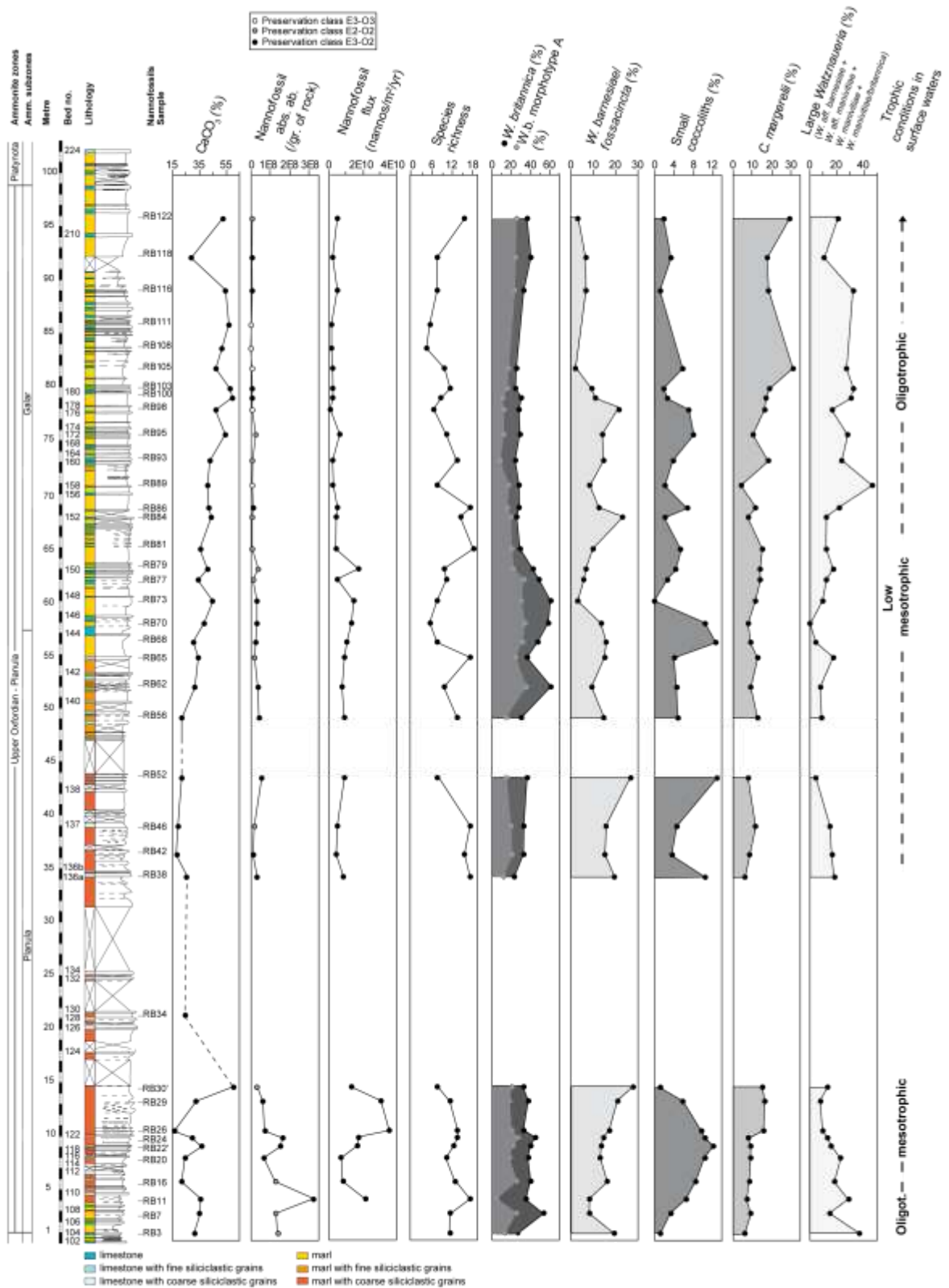
Fig. 5. Stratigraphic changes in calcium carbonate content, calcareous nannofossil total absolute abundance and flux, species richness, relative abundance of some selected taxa for the Ricla Barranco section. For discussion of trophic conditions refer to text.

for dissolution of carbonates and silicates, and saturated $ZnCl_2$ solution ($D \approx 2.2$ g/ml) for density separation. Residues were sieved at 15 µm mesh size. Slides have been mounted in Eukitt, a commercial, resin-based mounting medium.

For palynofacies analysis the sedimentary organic matter is grouped into a continental fraction including phytoclasts, pollen grains and spores, and a marine fraction composed of dinoflagellate cysts, acritarchs, prasinophytes and foraminiferal test linings. The relative percentage of these components is based on counting at least 400 particles per slide.

Three palynofacies parameters were calculated to detect stratigraphic changes in the composition of sedimentary organic matter reflecting eustatic signals: (1) the proportion of marine phytoplankton. This parameter quantifies the percentages of dinoflagellate cysts, acritarchs and prasinophytes in the sedimentary organic matter; (2) the ratio of opaque to translucent phytoclasts (OP/TR ratio). Opaque phytoclasts (OP) partly consist of charcoal originating from forest fires, but mainly develop by oxidation of translucent phytoclasts (TR). Another source for opaque phytoclasts might be resedimentation of refractory particles; and (3) the size and shape of plant debris (ED/BS ratio) are used to decipher proximal to distal and transgressive to regressive trends.

3.3. Calcareous nannofossils and calcimetry

A total of 37 rock samples were analysed both for their calcareous nannofossil abundances, assemblage composition and preservation, and for their calcium carbonate content (Fig. 5). Smear slides were prepared using the Geisen et al. (1999) random settling technique. This is a method adapted from Beaufort (1991) that allows the calculation of absolute abundances. Nannofossils were observed under a light polarising microscope at a magnification of $\times$ 1560. For the quantification, 150 to 300 specimens were counted in a variable number of fields of view on the smear slide. Due to the scarcity of nannofossils in the upper part of the succession, between 42 and 57 specimens were counted following several longitudinal transverses in four samples; in two samples (RB108 and RB111), nannofossils are too rare for the calculation of the relative abundance of species. The Bown and Cooper (1998) taxonomic framework was used. Two recent syntheses of Late Jurassic nannofossil schemes are available (de Kaenel et al., 1996; Bown and Cooper, 1998). The nannofossil preservation was evaluated following the classes defined by Roth (1983). The nannofossil absolute abundances are usually biased by dilution. Therefore, nannofossil fluxes were calculated by estimating the duration of recognized sedimentary sequences based on cyclostratigraphic calibration (see below). The nannofossil fluxes are expressed as F (number of nannofossils/m^2/yr) = "AA X r X sed. rate", with AA = nannofossil absolute abundance; r = volume mass of calcite (2.7 g.cm^{-3}) and sed. rate = sedimentation rate. The richness of species and the relative abundance of each identified species were also calculated. The calcium carbonate content was determined using the carbonate bomb technique, which measures CO_2 emission during a hydrochloric acid attack.

3.4. Clay mineralogy

Clay mineral associations were studied using X-ray diffraction (XRD) on oriented mounts. Oriented mounts were prepared as follows: the samples were decarbonated, and the clay fraction (< 2 μm) was separated by sedimentation and centrifugation using the Holtzapffel (1985) analytical procedure. X-ray diffractograms were obtained using a D2 Brucker diffractometer equiped with a LynxEye detector, with CuKα radiation and NI filter. Measurement parameters were as follows: 2.5 to 35 ° (2θ), step measurements of 0.02 ° (2θ) each 0.2 s. The identification of clay minerals was made according to the position of the (001) series of basal reflections of three X-ray diagrams, respectively obtained with non-treated, glycolated, and heated (450 °C, 4 hours) preparations (Brown and Brindley, 1980; Moore and Reynolds, 1989). Semi-quantitative evaluations are based on the peak areas estimated using
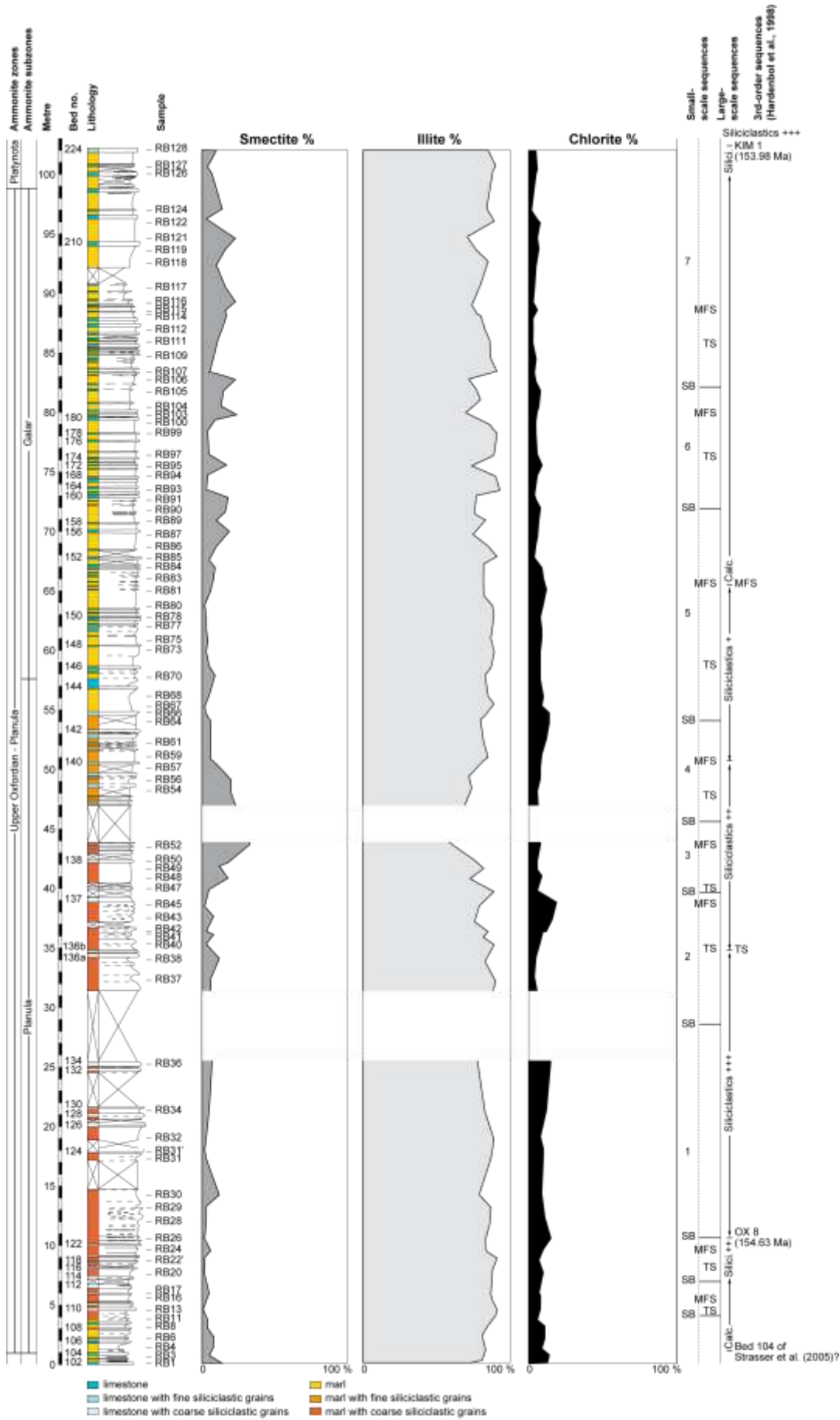
Fig. 6. Clay mineralogy of the Ricla Barranco section.

the Macdiff software. Areas were summed to 100 %, the relative error being 5 % (Holtzapffel, 1985). A total of 84 samples were analysed and the mean sample interval was 1.2 m (Fig. 6).

4. Results

4.1. Lithology, sedimentary and organic facies

The Ricla Barranco section has a thickness of 103 m (Fig. 3). The section is composed of six intervals, which are between 1 and 35 metres thick, and differ according to their content of siliciclastics (i.e., quartz, mica, clay). These intervals in turn contain marl-limestone alternations (or couplets), which are therefore either poor or rich in siliciclastic grains, depending on the interval in which they occur. Most of the limestone beds are wackestones, which include bivalves, echinoderms, foraminifers, serpulids, ostracodes, and wood debris (Fig. 3). The basal ten metres contain more siliciclastic grains in the upper part than in the lower part. This interval is characterised by numerous limestone beds and thin marl interbeds. The second interval, between 10 and 35 m, contains abundant covered parts, which are probably due to the decrease in the number of limestone beds and the increase in the marl interbed thickness. The increase in size and percentage of quartz adds to the increase in siliciclastics relative to carbonates. The interval between 35 and 50 m contains more limestone beds and thinner marl interbeds than the previous interval. Nevertheless, both size and percentage of quartz decrease only slightly, suggesting that the amount of siliciclastics remains high. This interval is also characterised by an increase in the percentage and in the size of mica. Between 50 and 65 m, the change from siliciclastic-rich alternations at the base to siliciclastic-poor alternations at the top and the decrease in the size of quartz and in the percentage of quartz and mica suggest a decrease in siliciclastics relative to carbonates. The interval between 65 and 103 m shows the same characteristics as the first interval, with the exception of the occurrence of solitary corals between 98 and 100 m. In the uppermost 13 m, the increase in the size and in the percentage of quartz and mica indicates an increase in siliciclastics relative to carbonates. Field observations show that this increase in siliciclastics continues above the studied section and results in a siliciclastic-rich interval.
Generally, sedimentary organic matter is poorly preserved throughout the studied section and dominated by phytoclasts (Fig. 4). However, the preservation of organic particles varies according to the lithology. Siliciclastic-rich intervals show a high content of terrestrial particles, mainly phytoclasts of different sizes and shapes, translucent and opaque. Calcareous intervals are characterised by the highest amount of marine phytoplankton, by small, equidimensional, opaque phytoclasts, and by a generally high percentage of degraded organic matter. The highest amount of degraded organic particles occurs within a calcareous interval between 65 and 72 m (samples RB83 to RB90). A decrease of blade-shaped opaque plant debris and large translucent particles corresponds to decreasing siliciclastics. An opposite trend is observed in the abundance of marine phytoplankton and small, opaque, equidimensional phytoclasts, reaching a maximum in the most calcareous interval.

4.2. Calcareous nannofossil biostratigraphy

All nannofossil taxa observed in the studied interval are reported in a table as Supplementary data. The Late Jurassic is marked by a differentiation between Boreal/Subboreal (NW Europe) and Tethyan (SW Europe and NW Atlantic Ocean) nannofossil assemblages leading to a reduction in the number of correlative bioevents (de Kaenel et al., 1996). *Watznaueria britannica* constitutes one of the principle components of

the assemblage (Bown et al., 1988; Bown and Cooper, 1998). Because of the absence of Oxfordian nannofossil biozones for the Tethyan realm, the nannofossil biozonation scheme defined for the northern Europe in Bown et al. (1988) is used in this study. The lower Oxfordian to lower Kimmeridgian interval corresponds to the nannofossil NJ15 Cyclagelosphaera margerelii Zone. This long zone, reflecting a period of evolutionary stasis, starts with the last occurrence (LO) of *Stephanolithion bigotii maximum* and ends with the first occurrence (FO) of *Stephanolithion brevispinus*. The NJ15 Zone is divided into two subzones. The NJ15a Lotharingius crucicentralis Subzone spans the LO of *S. bigotii maximum* to the LO of *L. crucicentralis*, and the NJ15b Hexapodorhabdus cuvillieri Subzone, defined by the LO of *L. crucicentralis* and the FO of *S. brevispinus* (Bown et al., 1988). The LO of *L. crucicentralis* occurs in the Upper Oxfordian and is correlated to the Regulare ammonite Zone in the Boreal area (Bown et al., 1988). *L. crucicentralis* becomes rare at the top of its range. This datum occurs in the Middle Oxfordian (Plicatilis ammonite Zone in SE France and Switzerland) (de Kaenel et al., 1996).

Other secondary but useful nannofossil events occur during the Upper Oxfordian to lowermost Kimmeridgian interval in Tethyan sections. The FO of *Microstaurus quadratus* is correlated to the base of the Bifurcatus Zone. The FO of *Faviconus multicolumnatus* is correlated to the top of the Bimammatum Zone. In southeast France, *Stephanolithion bigoti bigoti* becomes sporadic from the Upper Oxfordian onward (Bimammatum Zone, de Kaenel et al., 1996) but occurs until the Tithonian in the Iberian margin (de Kaenel and Bergen, 1996; Concheryo and Wise, 2001). In the Boreal realm, the LOs of *Discorhabdus striatus* and *Crepidolithus perforata* are recorded in the Glosense Zone (Middle–Upper Oxfordian) and Baylei Zone (lowermost Kimmeridgian), respectively. In the Ricla Barranco section, only one specimen of *L. crucicentralis* was observed (RB 84), *S. bigotii bigotii* are sporadic (one specimen in samples RB 42, RB 46, RB 65 and RB 81), two specimens of *D. striatus* were observed in RB 65, and one specimen of *C. perforata* in RB 38. *M. quadratus* and *F. multicolumnatus* were not observed. These data do not allow the distinction between the NJ15a and NJ15b subzones in the Ricla Barranco section.

4.3. Calcareous nannofossil assemblages and calcimetry

The nannofossil preservation is poor to moderate. Poorly-preserved assemblages are characterised by strongly etched and moderately or strongly overgrown specimens (categories E3 and O2, and E3 and O3 only for one sample); moderately-preserved assemblages are represented by moderately etched and overgrown specimens (categories E2 and O2). The nannofossil absolute abundance ranges from 2.1×10^6 to 3.2×10^8, with an average of 4.7×10^7 specimens/gram of rock (Fig. 5). Highest abundances are recorded at the base of the section, and the absolute abundance decreases upward. The nannofossil flux curve follows more or less the same trend as absolute abundance (Fig. 5). The highest nannofossil flux values are recorded in the lower part of the succession, between 10 and 15 m. In the middle part, from 35 to 65 m, the nannofossil fluxes are reduced in comparison to the lower part, with just a slight increase between 55 and 65 m. The lowest nannofossil flux values are recorded in the upper part of the succession. The species richness ranges from 5 to 19; it presents fluctuations but progressively decreases from 65 to 83 m (Fig. 5). Eight species represent between 80.8 and 100 % of the total nannofossil assemblage, which is composed of 45 species. The nannofossil assemblage is dominated by the genus *Watznaueria*, which comprises 50 to 93.6 % of the total assemblage. Amongst *Watznaueria*, *W. britannica* is the dominant species; other abundant taxa are in decreasing order of abundance: *W. barnesiae*, *Cyclagelosphaera margerelii*, *W.* aff. *barnesiae*, *Lotharingius hauffii*, *W.* aff. *manivitiae*, *W. manivitiae*. The seven morphotypes of *W. britannica* described in Giraud et al. (2006, 2009)

are present in the studied interval. *W. manivitiae/britannica* and *W.* aff. *barnesiae* were defined in Giraud et al. (2009). Groupings include *W. barnesiae*, *W. fossacincta*, which are believed to represent end-members of a morphological continuum (Lees et al., 2004, 2006; Bornemann and Mutterlose, 2006), small coccoliths (*Biscutum* spp., *Discorhabdus* spp., *D. lehmannii*, *L. hauffii*, and *Z. erectus*), with particular palaeoecological affinities in terms of trophic conditions, and the largest-sized *Watznaueria* (*W.* aff. *barnesiae*, *W. manivitiae*, *W.* aff. *manivitiae* and *W. manivitiae/britannica*). The relative abundances of *W. britannica* vary from 21.6 to 61.6 % and show a fairly marked increase in the middle part of the succession (between 49 and 64 m) (Fig. 5). This species is mostly represented by smallest-sized morphotype A (with an average of 56.3 % of the total number of *W. britannica*), which follows the same trend as the whole population of *W. britannica* (Fig. 5). The percentages of *Watznaueria barnesiae/fossacincta* fluctuate between 2 and 28 %; they increase and are the highest in the lower part of the section (below the major sedimentary gaps); they slightly decrease from 45 to 80 m, then they sharply decline in the upper part of the succession. The relative abundances of the small coccolith group vary from 0 to 13.1 % (Fig. 5). They increase to 9 m in the lower part of the succession and then decrease below the major gaps. Above the major gaps, their relative abundances are between 6 and 14 % below 60 m; they decrease in the upper part of the succession. The percentages of *C. margerelii* fluctuate between 4.2 and 31.4 % and higher values are recorded above 80 m (Fig. 5). The relative abundances of largest-sized *Watznaueria* range between 0 and 47 %; they decrease from the base to the top of the lower part of the succession (below the major gaps) (Fig. 5). The percentages of this group remain below 20 % in the middle part of the succession (from 35 to 68 m), and increase with values between 20 and 46.8 % in the upper part of the succession (from 68 to 91 m).

The calcium carbonate content ranges from 16.7 to 61 % (Fig. 5). In the lower part of the succession, between 1 and 15 m, it increases at the top of this interval. Above the major sedimentary gaps, the calcium carbonate content generally increases toward the top of the succession. Calcium carbonate content and nannofossil absolute abundance follow inverse trends (Fig. 5).

4.4. Clay mineralogy

The clay fraction is composed of illite (59 to 93 %), illite-smectite mixed layers (I/S, 1 to 33 %), and chlorite (2 to 19 %). The significant occurrences of smectitic minerals throughout the section exclude a major influence of burial diagenesis on clay mineral assemblages, as those minerals are the most sensitive to diagenetic processes (Chamley, 1989).

Smectite proportions generally increase from the lower to the upper part of the Ricla Barranco section (Fig. 6). Two smectite-enriched intervals are observed, the first one between 41 and 50 m, and the second one between 66 and 102 m. Smectite proportions average 19 % and 12 % in the first and second interval, respectively, whereas the average proportion equals 5 % in the rest of the section. The chlorite content decreases slightly but very regularly above 54 m, passing from 14 % in the lower part of the section to as low as 2 % in the upper part. A peak of chlorite occurs between 36 and 39 m, reaching as high as 19 % of all clay minerals. This peak occurs just below the first smectite-enriched interval.

5. Interpretations

5.1. Sedimentary and organic facies

During the late Oxfordian, the study area was located south of the Ebro Massif, which furnished siliciclastics (Fig. 1). Siliciclastics reached this area through a delta plain (Aurell and Meléndez 1993, p. 354), which shifted basinward during periods of tectonic uplift of marginal areas (Aurell, 1991, p. 111; Aurell and Bádenas, 1994, p. 92). High terrestrial input via delta systems is also documented by the high amount of plant debris. Phytoclasts are the dominant group of sedimentary organic particles. Their highest variability in size and shape occurs in siliciclastic-rich intervals (Fig. 4). Carbonates formed seaward, in the open-marine realm (Aurell et al., 1998, p. 159). The proportion of marine phytoplankton is linked to the marine conditions of the water column, depending on distance to coastline, water depth, temperature, salinity, and nutrient availability. Generally, the ratio of opaque to translucent phytoclasts increases basinward due to fractionation processes and the higher preservation potential of opaque particles (Summerhayes, 1987; Tyson, 1993; Pittet and Gorin, 1997; Bombardière and Gorin, 1998). Most of the oxidation is of subaerial, continental origin (Tyson, 1995). However, in proximal high-energy shelf areas this trend may be reversed by in-situ (bio)oxidation at the seafloor (Batten, 1982; Boulter and Riddick, 1986; Bustin, 1988; Tyson, 1993), enhanced by the high porosity and permeability of coarse-grained sediments (Tyson, 1993). Small, equidimensional (ED) woody fragments are characteristic of distal deposits, whereas in proximal settings, large blade-shaped (BS) particles are quite abundant (Steffen and Gorin, 1993; Götz et al., 2008; Haas et al., 2010). In addition, proximal assemblages reveal a greater variety of particle sizes and shapes (Tyson, 1993; Tyson and Follows, 2000; Götz et al., 2008; Haas et al., 2010). In the Ricla Barranco section, maximum abundances of marine phytoplankton, foraminiferal test linings and equidimensional, opaque phytoclasts and a high amount of degraded organic particles point to a distal, open-marine depositional environment. Moreover, transport characteristics of quartz and mica are different. High percentages of coarse quartz indicate well-winnowed environments while high percentages of mica are characteristic of lower energy environments (Doyle et al., 1968; 1983 in Pettijohn et al., 1987, p. 38). Flakes of mica tend to be winnowed out of high-energy environments by turbulence and strong currents, and carried away toward more distal areas. Consequently, carbonates in the Ricla Barranco section, which contain maximum abundances of marine phytoplankton, foraminiferal test linings and equidimensional, opaque phytoclasts and a high amount of degraded organic particles, indicate more distal environments than siliciclastics in which phytoclasts dominate. Within siliciclastic-rich intervals, high percentages of coarse grains of quartz indicate more proximal environments than high percentages of mica.

5.2. Sequence and cyclostratigraphy

The above described stratal facies patterns indicate that the evolution through time of siliciclastic and phytoclast inputs reflect changes in depositional environment. These changes in environment depended on relative sea-level variations and can be interpreted as sequences. At outcrop scale, the most siliciclastic intervals (i.e., between 10 and 35 m, and just above the studied section) probably represent large-scale lowstand deposits (LSDs), whose bases coincide with sequence boundaries (SBs), and tops with transgressive surfaces (TSs) (Fig. 3). This interval is dominated by opaque plant debris (samples RB26 to RB38). The most calcareous intervals (i.e., the first 10 m and between 65 and 103 m) probably document large-scale highstand deposits (HSDs), which formed above maximum-flooding surfaces (MFSs)

and below SBs. Maximum abundance of marine phytoplankton, foraminiferal test linings and opaque, equidimensional phytoclasts occurs in an interval from bed 151 to bed 159 (samples RB83 to RB90), marking maximum flooding (Fig. 4). The early highstand phase is identified within an interval spanning beds 160 to 180 (samples RB93 to RB100), showing a still high amount of marine phytoplankton and opaque, equidimensional phytoclasts. Late highstand deposit are characterised by decreasing marine phytoplankton and a higher amount of translucent, large blade-shaped particles than before. The transgressive deposit (TSD) is recorded by the siliciclastic-rich interval between 35 and 65 m (samples RB40 to RB81), showing an overall increase in marine phytoplankton and equidimensional, opaque phytoclasts (Fig. 3, 4).

This large-scale sequence, which is located between 10 and 103 m, allows the definition of the diagnostic criteria for the recognition of smaller-scale stratigraphic surfaces. The most pronounced surfaces are TSs and MFSs. TSs correspond to the highest quartz percentages, whereas the highest mica percentages indicate MFSs (Fig. 3). The base of the thickest marl interbeds probably indicates SBs, which often correspond to covered intervals. Small-scale cyclicity is also documented in palynofacies by peak abundance of marine phytoplankton (samples RB16, RB22, RB32, RB43, RB52, RB57, RB72, RB95, RB100, RB109, RB116) indicating small-scale MFSs and TSs (Fig. 4). Based on these diagnostic criteria, at least 7 small-scale sequences have been defined in the large-scale sequence described above. These small-scale sequences are 10 metres thick on average.

The studied interval corresponds to the Planula Zone (Figs. 2, 3). Its lower boundary is located 9 m below the first large-scale sequence boundary (SB), its upper boundary, at least 2 to 3 m below the second large-scale SB (Bádenas et al., 1998; Delvene, 2001). Based on this biostratigraphic dating, the first large-scale SB corresponds to the third-order SB Ox 8 defined by Hardenbol et al. (1998), and the upper boundary to the third-order SB Kim 1 (Fig. 2). According to Hardenbol et al. (1998), which is the only chronostratigraphic chart drawing a parallel between sequence stratigraphy, ammonite zonation and geological time scale, the duration of this interval is 650 kyr (between 154.63 and 153.98 Ma) (Fig. 2). More recent geological time scales (i.e., Gradstein et al., 2004; Ogg et al., 2008; Gradstein et al., 2012) follow the sequence-stratigraphical interpretation of Hardenbol et al. (1998). Small-scale sequences would therefore have lasted around 93 kyr. This suggests that orbital cycles (in this case the short eccentricity cycle of 100 kyr) influenced the sedimentation during the latest Oxfordian. This interpretation is consistent with the results of Strasser et al. (2005) who analysed a section that lies just below the interval studied here.

5.3. Calcareous nannofossil assemblages

W. britannica, *W. barnesiae/fossacincta* and *C. margerelii* are considered as *r*-strategists that can live in unstable environments (Lees et al., 2005, 2006). The smallest-sized specimens of *W. britannica* (Morphotype A) are characteristic of turbulent, unstable environmental conditions and/or eutrophic levels, whereas large-sized morphotypes were adapted to stable and more oligotrophic conditions (Giraud, 2009; Giraud et al., 2009). *W. barnesiae* is considered a eurytopic taxon for the Jurassic and Cretaceous period (Mutterlose, 1991), indicative of mesotrophic conditions in the Jurassic (Pittet and Mattioli, 2002). *C. margerelii* reflects low mesotrophic conditions (Pittet and Mattioli, 2002) and can become dominant in neritic and/or restricted environments (Bown, 2005; Giraud et al., 2005; Carcel et al., 2010). *L. hauffii* is a marker of meso-eutrophic conditions (Pittet and Mattioli, 2002) and can be abundant in proximal eutrophic environments (Mattioli, 2006). Small coccoliths such as *Biscutum* spp., *Discorhabdus* spp., *D. lehmannii*, *Z. erectus* are markers of high surface-water fertility for the Jurassic and Cretaceous (Roth, 1981; Roth and Bowdler, 1981; Roth and

Krumbach, 1986; Premoli Silva et al., 1989; Erba, 1992; Coccioni et al., 1992; Williams and Bralower, 1995; Mattioli and Pittet, 2004), but were probably not competitive with respect to the dominant smaller-sized *W. britannica* in unstable and eutrophic surface waters for the Middle and Late Jurassic (Giraud, 2009; Giraud et al., 2009). Amongst the large-sized *Watznaueria*, *W. manivitiae* is indicative of oligotrophic conditions (Pittet and Mattioli, 2002); *W. manivitiae/britannica* could have a preference for proximal environments and/or high productivity in surface waters (Giraud et al., 2009). Nutrients for nannofossils can be delivered from the emerged continents to the basin via an intensified runoff, or from upwellings. Low to high content of nutrients correspond to oligotrophic to eutrophic conditions, respectively.

Considering the ecological affinities of the most abundant taxa encountered in the Ricla Barranco section, the successive palaeoecological conditions are the following (Fig. 5): the first part of the section (below the major gaps) can be divided into three parts: from 0 to 4 m, the dominance of the large-sized *Watznaueria* group and the low relative abundance of small coccoliths suggest oligotrophic conditions; from 4 to 10 m, fertility of the surface waters increases as indicated by the increase in abundance of small coccoliths; from 10 to 15 m, the increase in both the nannofossil fluxes and the relative abundance of *W. barnesiae/fossacincta* and *C. margerelii* suggests mesotrophic conditions. Above the gap, from 35 to 49 m, the lower nannofossil flux values, but still higher relative abundances of small coccoliths in comparison to the preceeding interval, suggest low mesotrophic conditions in surface waters. From 49 to 63 m, the increase in the relative abundance of smallest-sized *W. britannica* can be indicative of higher trophic conditions in comparison to the preceeding interval, also attested by higher nannofossil fluxes. In the upper part of the succession (until 90 m), the sharp increase in the relative abundances of large-sized *Watznaueria* and the decrease in both nannofossil fluxes and relative abundances of small coccoliths (*W. britannica* Morphotype A included) indicate that oligotrophic conditions prevailed in surface waters. Toward the top of the succession (above 80 m), the increase in the relative abundance of *C. margerelii* could be indicative of more proximal and or more restricted conditions in comparison to the rest of the succession.

5.4. Clay mineralogy

Clay mineral trends at Ricla Barranco match well with the changes in microfacies and carbonate content of the rocks and in calcareous nannofossil assemblages. Predominating illite minerals throughout the studied section and rather high proportions of chlorite in the lower part of the section testify to a generally high erosional activity and high detrital input from land (Chamley, 1989). The peak of chlorite between 36 and 39 m and the first smectite-enriched interval between 41 and 50 m correspond to the highest percentages of quartz and of micas, the coarsest micas, and coarse quartz as revealed by the thin section analysis and to the lowest carbonate percentages (Figs. 3, 5, 6). These mineralogical changes and the high detrital signature are most probably related to the relatively shallow setting of Ricla Barranco on the ramp, the neighbouring Ebro Massif providing the clastic input to this area (Fig.1, Bádenas and Aurell, 2001; Aurell et al., 2003), and the extensional tectonic activity that affected the sedimentation during the Late Jurassic in this part of the Iberian basin (Bádenas and Aurell, 2001).

The generally low smectite and relatively high chlorite proportions below 66 m are parallel with low or moderate carbonate content, mostly mesotrophic to low mesotrophic conditions as indicated by calcareous nannofossils, and high siliciclastic content of the rock (high quartz and mica percentages and sizes) (Figs. 3, 5, 6). On the contrary, the generally high smectite and relatively low chlorite proportions above 66 m are associated with

increasing carbonate content, oligotrophic conditions, and low quartz and mica percentages. These conditions develop near the Planula–Galar Subzone boundary, and persist until the occurrence of solitary corals between 98 and 100 m. A new siliciclastic-rich interval begins in the last 13 meters of the studied section (Fig. 3, 5). The generally increasing I/S and decreasing chlorite proportions up-section most probably reflect a transition from humid to drier climates during the Planula Zone. Interestingly, no kaolinite was found among the clay minerals at Ricla Barranco. This suggests a generally dry regional climate and poorly drained soils. High relative sea level during the upper Planula and the lower Galar subzones may have led to reworking of smectitic-rich soils on the shores of the Iberian Massif (Pellenard and Deconinck, 2006).

6. Discussion

6.1. Reconstructions of palaeoenvironmental, palaeoclimatic, and tectonic changes and timing of these events

As stated in the present work, major changes in sedimentological, micropalaeontological, and mineralogical data were recorded on the Iberian ramp during the latest Oxfordian. They are interpreted in terms of variations in palaeoenvironmental and palaeoclimatic conditions and in tectonic activity taking place in the period of time in three key steps (Figs. 7, 8). The definition of small-scale (100 kyr) sedimentary sequences, based on sequence and cyclostratigraphy, enables to specify the timing of these changes and their succession throughout the Planula Zone (Fig. 8). Both nannofossil and clay mineral assemblages allow the reconstruction of the trophic and climatic conditions prevailing during the latest Oxfordian. Palaeotemperatures are from Brigaud et al. (2008). During the first 300 kyr of the Planula Subzone (i.e., before step 1), the highest abundances of small coccoliths, the predominance of illite and high proportions of chlorite, along with the gradually increasing size and content of quartz and corresponding decreasing percentage of carbonate testify to increasing surface-water fertility in proximal shallow-marine environments due to increasing siliciclastic and nutrient input from land (Figs. 7, 8). These palaeoenvironmental conditions probably resulted from the highstand prograding wedge that formed just before third-order sequence boundary Ox 8, and from relatively humid climatic conditions, as shown by the clay mineral assemblages (Fig. 8). In the upper part of the Planula Subzone, the greater abundance of quartz, muscovite, and clay relative to the lower part of that Subzone testifies to the enhanced tectonic activity, which has been identified in the Iberian basin during this period. This enhanced tectonic activity would have lasted 200 kyr (Fig. 8), and might be partly responsible for the relative sea-level rise observed from the middle part of the Planula Subzone (i.e., third-order sequence boundary Ox 8) to the lower part of the Galar Subzone (i.e., maximum flooding of the Ox 8 sequence, after step 2) (Figs. 7, 8). This sea-level rise probably explains both the increase in the water energy, as revealed by the highest abundances of degraded organic particles and of the smallest-sized *W. britannica*, and the decrease in siliciclastics. Indeed, the climatic conditions remained as humid as before; Brigaud et al. (2008) indicate a slight increase in temperature. Major palaeoenvironmental and palaeoclimatic changes take place after the transition between the Planula and the Galar subzones (i.e., step 3) (Figs. 7, 8). This transition first precedes both small- and large-scale maximum flooding (Figs. 3, 8). Then, around this boundary and during the following sea-level highstand, interbeds become more calcareous than before, as attested by the increase in carbonate content. However, the thickness of the calcareous beds remains the same, suggesting that the carbonate factory was not more active than in the lower and the middle
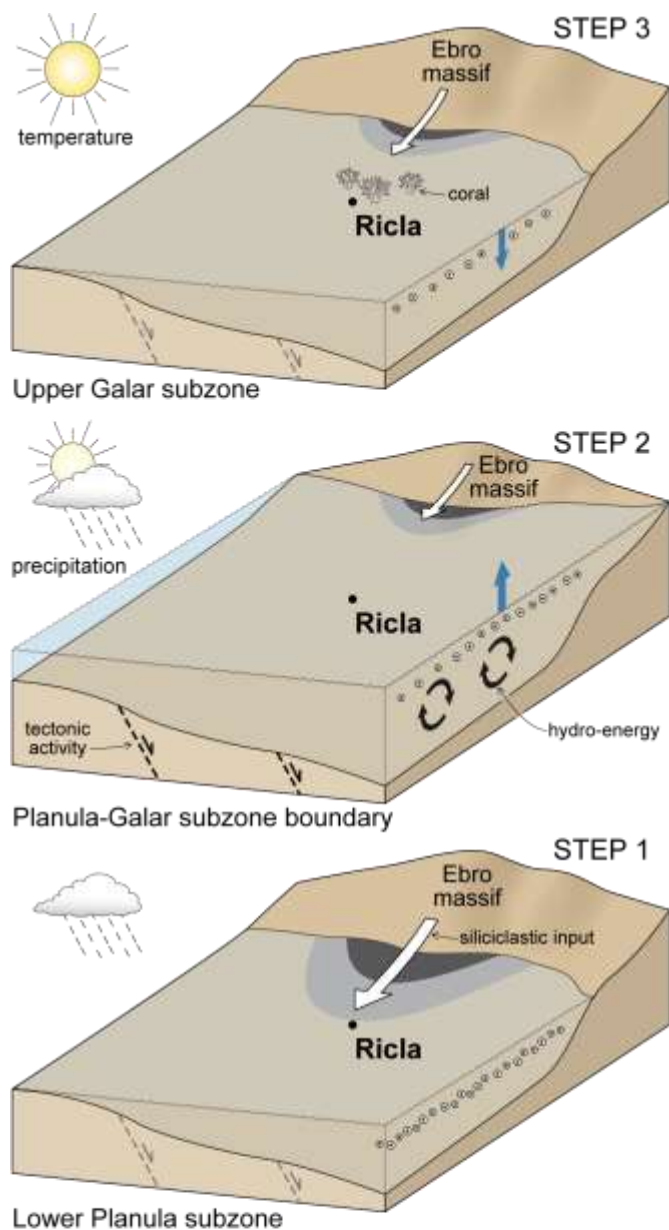
Fig. 7. Three-dimensional representation of the three key steps in the palaeoenvironmental evolution of the Ricla area during the Planula ammonite Zone, including the Planula and the Galar subzones. Step 1, lower part of the Planula Subzone: high silicilastic input related to large extension of deltaic facies under humid climatic conditions during slightly falling relative sea level. Step 2, Planula–Galar subzones boundary: decreasing siliciclastics associated with high relative sea level under slightly warmer but still humid climatic conditions. High sea level leads to more open-marine environments and higher water energy. These environmental conditions develop just after a period of enhanced tectonic activity. Step 3, upper part of the Galar Subzone: climatic conditions become drier and warmer than before. Oligotrophic sea-surface conditions lead to some coral growth. Phytoplankton dots: small dots correspond to small coccoliths with dominance of smallest-sized W. britannica, whereas larger dots correspond to bigger coccoliths such as largest-sized W.britannica.
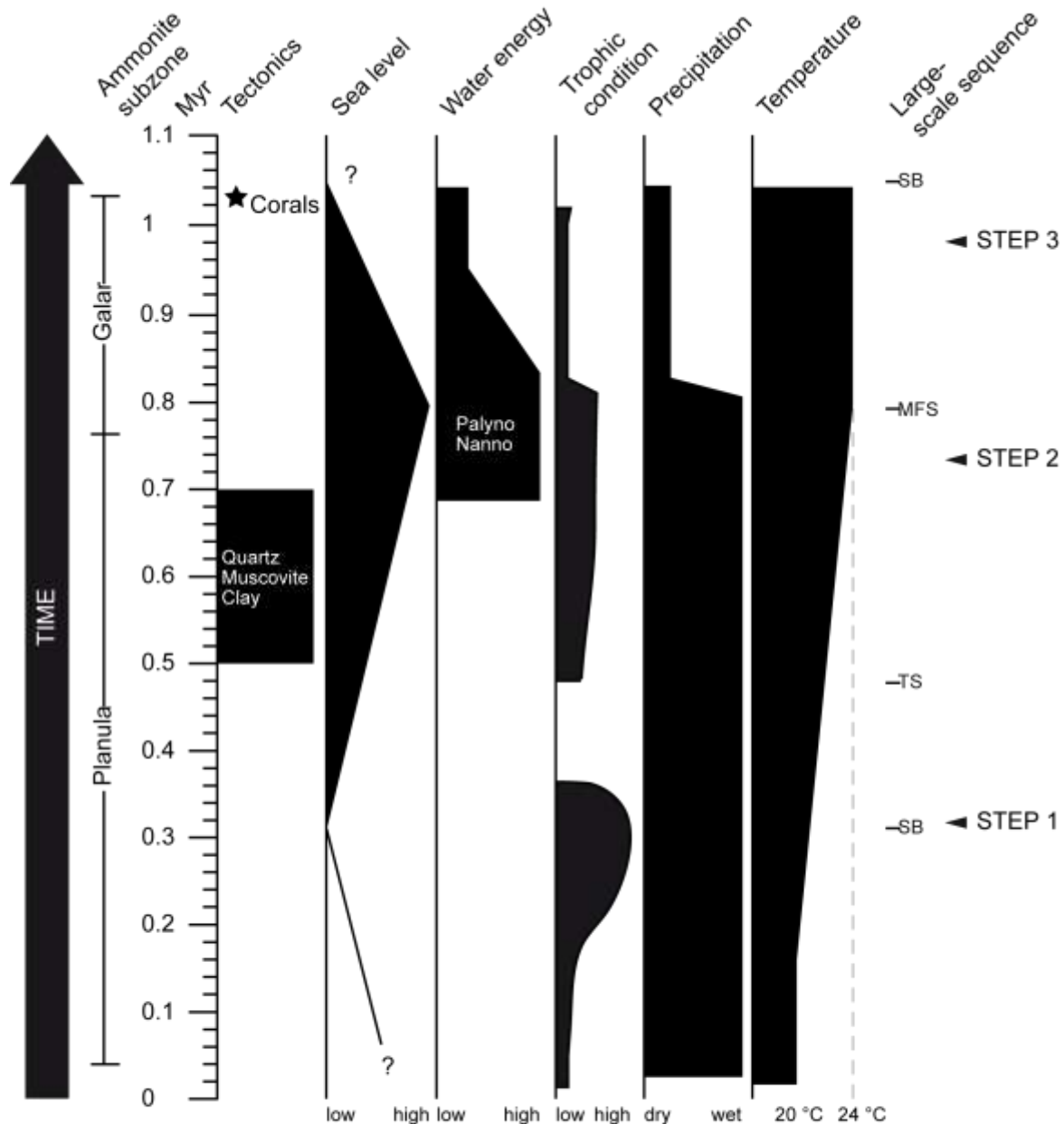
Fig. 8. Stratigraphic distribution of major tectonic, palaeoenvironmental and palaeoclimatic events recorded in the Ricla Barranco section during the Planula Zone. Palaeotemperature data in the Paris basin are from Brigaud et al. (2008). See text for detailed explanations.

parts of the section studied, but that siliciclastic input was lower. The fertility of sea-surface waters changed from mesotrophic at the Planula–Galar Subzone boundary to oligotrophic during the Galar Subzone interval. The decrease in the nannofossil primary productivity suggests less nutrient input from land than before. The decrease in siliciclastics and associated nutrients and the lowest chlorite and the highest smectitic percentages imply that the climate was less humid than before (Fig. 7).

6.2. Contribution of the Iberian ramp high-resolution data to the knowledge of the Oxfordian-Kimmeridgian boundary palaeoclimate

19

Drier climatic conditions from the Planula–Galar Subzone transition match well with increasing aridity recognised in the North Sea basin (Abbink et al., 2001), the Swalbian Alb deep shelf (SW Germany, Bartolini et al., 2003), and the shallow platforms of the Jura Mountains and of Spain (Pittet et al., 2000; Colombié, 2002; Hug, 2003; Colombié and Strasser, 2005) at the Oxfordian to Kimmeridgian transition. Interestingly, as mentioned earlier, no kaolinite is recorded during the Oxfordian–Kimmeridgian transition at Ricla Barranco, whereas kaolinite occurs in variable amounts in contemporaneous sediments from the Paris basin (i.e., in Normandy, see Saint-Germès et al., 1996, in the Boulonnais area, see Schnyder et al., 2000, and in the eastern part, see Brigaud et al., 2014). Brigaud et al. (2014) showed that these humid conditions at the Oxfordian–Kimmeridgian boundary could be at least partly responsible for the decline of carbonate production in these areas. This shows that relatively more humid climates would have occurred at latitudes that were more northern than the Iberian basin during this transition.

Using oxygen-isotope data measured on oyster shells in the Paris basin, Brigaud et al. (2008) identified a warming trend of about 7 °C from the Upper Oxfordian Bimmamatum Zone to the early Kimmeridgian. These detailed palaeoclimatic fluctuations from the Oxfordian to the early Kimmeridgian are supported by palynological data from the North Sea basin (Abbink et al., 2001), which show a warm and dry phase at the Oxfordian–Kimmeridgian transition. In Ricla Barranco, both the warming and the drier conditions, which favoured oligotrophy as demonstrated by nannofossil assemblages, probably explain the occurrence of solitary corals at the top of the interval studied (Figs. 7, 8). Cecca et al. (2005) and Martin-Garin et al. (2012) observed high coral abundance in the Tethyan and Peri-Tethyan realms during the late Oxfordian, highlighting a general warming. They also interpreted the higher coral diversity found at a more southerly position (when compared to the middle Oxfordian) as to be at least partly related to southward displacement of the anticyclonic zone to around 25° N latitude, which is the position of the Iberian ramp at this time (Osete et al., 2011 in Bádenas et al., 2012).

The palaeoclimatic results deduced from the study of the Ricla Barranco section are thus in accordance with the model of southward/northward moving atmospheric convective cells as suggested by Cecca et al. (2005) and explained by Martin-Garin et al. (2012).

7. Conclusions

The analysis of sedimentary facies, palynofacies, calcareous nannofossils and clay mineral assemblages in the uppermost Oxfordian (Planula and Galar subzones) of the Ricla Barranco section (northeastern Spain) has led to a detailed reconstruction of climatic, oceanographic, and tectonic processes that ruled the depositional environment.

Changes in sedimentary and organic facies allow the definition of one large-scale and 7 small-scale sequences. On the basis of the hierarchical stacking-pattern of these sequences and the available ammonite zonation for the interval studied, the first and the second large-scale sequence boundaries correlate with the Hardenbol et al. (1998) third-order sequence boundaries Ox 8 and Kim 1, respectively. Each of the small-scale sequences lasted 100 kyr, which implies a control by the short eccentricity cycle.

The nannofossil abundances and fluxes and the relative abundances of large-sized *Watznaueria* are higher in the upper part than in the lower part of the interval studied, suggesting a decrease in sea-surface trophic conditions, from mesotrophic at the Planula–Galar Subzone boundary to oligotrophic during the Galar Subzone interval. The decrease in the nannofossil primary productivity in the upper part of the interval studied suggests less

nutrient input from land than before. A long-term increase in smectitic minerals and a decrease in chlorite during the Galar Subzone interval suggest the development of drier climatic conditions than before, leading to a decrease in siliciclastic input and an increase in carbonate deposition.

The peak of chlorite and the smectite-enriched interval of the upper part of the Planula Subzone and the associated detrital (quartz and mica) input are interpreted as reflecting a tectonic pulse (namely the local expression of the onset of the Late Jurassic to Early Cretaceous rifting stage). According to the high-resolution chronostratigraphic framework established in this work, this major tectonic event would have occurred just before the Planula–Galar Subzone boundary, 300 kyr before the recovery of carbonate deposition. This return toward optimum conditions for carbonate sedimentation corresponds to increasing global sea level and decreasing rainfall in the hinterland.

Acknowledgements

References

Abbink, O., Targarona, J., Brinkhuis, H., Vissher, H., 2001. Late Jurassic to earliest Cretaceous palaeoclimatic evolution of the southern North Sea. Global Planet. Change 30, 231–256.

Alvaro, M., Capote, R., Vegas, R., 1978. Un modelo de evolucion geotectonica para la Cadena Celtiberica. Acta Geologica Hispanica 14, 172–177.

Aurell, M., 1990. El Jurásico Superior en la Cordillera Ibérica Central provincias de Zaragoza y Teruel). Análisis de cuenca. Ph.D. Thesis, University of Zaragoza, 389 pp.

Aurell, M., 1991. Identification of systems tracts in low angle carbonate ramps: examples from the Upper Jurassic of Iberian Chain (Spain). Sedimentary Geology 73, 101–115.

Aurell, M., Meléndez, A., 1993. Sedimentary evolution and sequence stratigraphy of the Upper Jurassic in the central Iberian Chain, northeast Spain, in: Possamentier, H.W. et al. (Eds.), Sequence Stratigraphy and facies associations. Int. Assoc. Sediment., Spec. Pub. 18, pp. 343–368.

Aurell, M., Bádenas, B., 1994. Facies and depositional sequence evolution controlled by high-frequency sea-level changes in a shallow-water carbonate ramp (late Kimmeridgian, NE Spain). Geol. Mag. 141, 717–733.

Aurell, M., Bosence, D., Waltham, D., 1995. Carbonate ramp depositional systems from a late Jurassic epeiric platform (Iberian Basin, Spain): a combined computer modelling and outcrop analysis. Sedimentology 42, 75–94.

Aurell, M., Bádenas, B., Bosence, D.W.J., Waltham, D.A., 1998. Carbonate production and offshore transport on a Late Jurassic carbonate ramp (Kimmeridgian, Iberian basin, NE Spain): evidence from outcrops and computer modelling, in: Wright, V.P, Burchette, T.P (Eds.), Carbonate ramps. Geol. Soc. Lon., Spec. Public. 149, pp. 137–161.

Aurell, M., Robles, S., Bádenas, B., Rosales, I., Quesada, S., Meléndez, G., García-Ramos, J.C., 2003. Transgressive- regressive cycles and Jurassic palaeogeography of northeast Iberia. Sediment. Geol., 162, 239–271.

Aurell, M., Bádenas, B., Ipas, J., Ramajo, J., 2010. Sedmentary evolution of an Upper Jurassic carbonate ramp (Iberian Basin, NE Spain), in: van Buchem, F., Gerdes, K., Esteban, M. (Eds.), Reference models of Mesozoic and Cenozoic carbonate systems in Europe and the Middle East — stratigraphy and diagenesis, Geol. Soc. Lon., Spec. Public. 329, pp. 87–109.

Baccelle, L., Bosellini, A., 1965. Diagrammi per la stima visiva della composizione percentuale nelle rocce sedimentarie. – Annali della Università di Ferrara, Sezione IX, Science Geologiche e Paleontologiche 1, 59–62.

Bádenas, B., Aurell, M., Pérez-Urresti, I., Delvene, G., 1998. Estratigrafía y evolución sedimentaria del Oxfordiense superior–Titónico inferior en Ricla (Zaragoza). Geogaceta, 24, 35–38.

Bádenas, B., Aurell, M., 2001. Kimmeridgian palaeogeography and basin evolution of northeastern Iberia. Palaeogeogr. Palaeoclimatol. Palaeoecol. 168, 291–310.

Bádenas, B., Pomar, L., Aurell, M., Morsilli, M., 2012. A facies model for internalites (internal wave deposits) on a gently sloping carbonate ramp (Upper Jurassic, Ricla, NE Spain). Sediment. Geology 271-272, 44–57.

Bartolini, A., Pittet, B., Mattioli, E., Hunziker, J.C., 2003. Shallow-platform palaeoenvironmental conditions recorded in deep-shelf sediments: C and O stable siotopes in Upper Jurassic sections of southern Germany (Oxfordian-Kimmeridgian). Sediment. Geology 160, 107–130.

Batten, D.J., 1982. Palynofacies, palaeoenvironments, and petroleum. J. Micropalaeontol. 1, 107–114.

Beaufort, L., 1991. Adaptation of the random settling method for quantitative studies of calcareous nannofossils. Micropalaeontology 37, 415–418.

Bombardière, L., Gorin, G.E., 1998. Sedimentary organic matter in condensed sections from distal oxic environments: examples from the Mesozoic of SE France. Sedimentology 45, 771–788.

Bornemann, A., Mutterlose, J., 2006. Size analyses of the coccolith species *Biscutum constans* and *Watznaueria barnesiae* from the Late Albian "Niveau Breistroffer" (SE France): taxonomic and palaeoecological implications. Geobios 39, 599–615.

Boulter, M.C., Riddick, A., 1986. Classification and analysis of palynodebris from the Palaeocene sediments of the Forties Field. Sedimentology 33, 871–886.

Bown, P.R., 2005. Selective calcareous nannoplankton survivorship at the Cretaceous-Tertiary boundary. Geology 33, 653–656.

Bown, P.R., Cooper, M.K.E., Lord, A.R., 1988. A calcareous nannofossil biozonation scheme for the early to mid Mesozoic. Newsl. Stratigr. 20, 91–114.

Bown, P.R., Cooper, M.K.E., 1998. Jurassic, in: Bown, P.R. (Ed.), Calcareous Nannofossil Biostratigraphy. British Micropalaeontological Society Series, Kluwer Academic Press, Dordrecht, pp. 34–85.

Brigaud, B., Pucéat, E., Pellenard, P., Vincent, B., Joachimski, M.M., 2008. Climatic fluctuations and seasonality during the Late Jurassic (Oxfordian-Early Kimmeridgian) inferred from $\delta^{18}O$ of Paris Basin oyster shells. Earth Planet. Sc. Lett. 273, 58–67.

Brigaud, B., Vincent, B., Carpentier, C., Robin, C., Guillocheau, F., Yven, B., Huret, E., 2014. Growth and demise of the Jurassic carbonate platform in the intracratonic Paris Basin (France): Interplay of climate change, eustasy and tectonics. Mar. Petrol. Geol. 53, 3–29.

Brown, G., Brindley, G.W., 1980. X-ray diffraction procedure for clay mineral identification, in : Brindley, G.W., Brown G. (Eds.), Crystal structures of clay minerals and their X-ray identification. London, Mineral. Soc. Monogr. 5, 305–359.

Bustin, R.M., 1988. Sedimentology and characteristics of dispersed organic matter in Tertiary Niger Delta: origin of source rocks in a deltaic environment. Am. Assoc. Petrol. Geol. Bull. 72, 277–298.

Carcel, D., Colombié, C., Giraud, F., Courtinat, B. 2010. Tectono-eustatic control on a mixed siliciclastic-carbonate platform during Kimmeridgian (La Rochelle platform, western France). Sediment. Geology 223, 334–359.

Catuneanu, O., Abreu, V., Bhattacharya, J.P., Blum, M.D., Dalrymple, R.W., Eriksson, P.G., Fielding, C.R., Fisher, W.L., Galloway, W.E., Gibling, M.R., Giles, K.A., Holbrook, J.M., Jordan, R., Kendall, C.G.St.C., Macurda, B., Martinsen, O.J., Miall, A.D., Neal, J.E., Nummedal, D., Pomar, L., Posamentier, H.W., Pratt, B.R., Sarg, J.F., Shanley, K.W., Steel, R.J., Strasser, A., Tucker, M.E., Winker, C., 2009. Towards the standardization of sequence stratigraphy. Earth-Sci. Rev. 92, 1–33.

Catuneanu, O., Galloway, W.E., Kendall, C.G.St.C., Miall, A.D., Posamentier, H.W., Strasser, A., Tucker, M.E., 2011. Sequence Stratigraphy: Methodology and Nomenclature. Newsl. Stratigr. 44, 173–245.

Cecca, F., Martin-Garin, B., Marchand, D., Lathuilière, B., Bartolini, A., 2005. Paleoclimatic control of biogeographic and sedimentary events in Tethyan and peri-Tethyan areas during the Oxfordian (Late Jurassic). Palaeogeogr. Palaeoclimatol. Palaeoecol. 222, 10–32.

Chamley, H., 1989. Clay Sedimentology, Springer Verlag, 623 pp.

Coccioni, R., Premoli Silvá, I., Erba, E., 1992. Barremian-Aptian calcareous plankton biostratigraphy from the Gorgo Cerbara section (Marche, central Italy) and implications for plankton evolution. Cretaceous Res. 13, 517–537.

Colombié, C., 2002. Sédimentologie, stratigraphie séquentielle et cyclostratigraphie du Kimméridgien du Jura suisse et du Bassin vocontien (France) : relations plate-forme – bassin et facteurs déterminants. GeoFocus 5, Fribourg, 201 pp.

Colombié, C., Strasser, A., 2005. Facies, cycles, and controls on the evolution of a keep-up carbonate platforms (Kimmeridgian, Swiss Jura). Sedimentology 52, 1207–1227.

Concheryo, A Wise, S.W., Jr., 2001. Jurassic calcareous nannofossils from prerift sediments drilled during ODP Leg 173, Iberia Abyssal Plain, and their implications for rift tectonics, in: Bellier, M.-O., Whitmarsh, R.B., Wallace, P.J., Girardeau, J. (Eds.), Proc. ODP, Sci Results 173, pp. 1–24.

Delvene, G., 2001. Los bivalves del Jurásico Medio y Superior en la Cordillera Iberica (Espanã) : sistematica y Paleoecologia-Tesis Doct, Univ, Zaragoza, Dept. C. Tierra, 209 pp.

Dromart, G., Garcia, J.P., Gaumet, F., Picard, S., Rousseau, M., Atrops, F., Lecuyer, C., Sheppard, S.M.F., 2003. Perturbation of the carbon cycle at the Middle/Late Jurassic transition: geological and geochemical evidence. Am. J. Sci. 303, 667–707.

Doyle, L.J., Clearly, W.J., Pilkey, O.H., 1968. Mica: its use in determining shelf-depositional regimes. Mar. Geol. 6, 381–389.

Doyle, L.J., Carder, K.L., Steward, R.G., 1983. The hydraulic equivalence of mica. J. Sediment. Petrol. 53, 643–648.

Erba, E., 1992. Calcareous nannofossil distribution in pelagic rhythmic sediments (Aptian Albian Piobbico core, central Italy). Rivista Italiana Paleontologia Stratigraphica 97, 455–484.

Geisen, M., Bollmann, J., Herrle, J.O., Mutterlose, J., Young, J.R., 1999. Calibration of the random settling technique for calculation of absolute abundances of calcareous nannoplankton. Micropaleontology 45, 437–442.

Giraud, F., 2009. Calcareous nannofossil productivity and carbonate production across the Middle-Late Jurassic transition in the French Subalpine basin. Geobios, 42, 699–714.

Giraud, F., Courtinat, B., Garcia, J.P., Baudin, F., Guillocheau, F., Dromart, G., Atrops, F., Colleté, C., 2005. Palynofacies and calcareous nannofossils in the Upper Kimmeridgian, southeastern Paris Basin (France). Bull. Soc. géol. Fr. 176, 457–466.

Giraud, F., Pittet, B., Mattioli, E., Audouin, V., 2006. Paleoenvironmental controls on morphology and abundance of the coccolith *Watznaueria britannica* (Late Jurassic, southern Germany). Mar. Micropaleontol. 60, 205–225.

Giraud, F., Courtinat, B., Atrops, F., 2009. Spatial distribution patterns of calcareous nannofossils across the Callovian-Oxfordian transition in the French Subalpine basin. Mar. Micropaleontol. 72, 129–145.

Götz, A.E., Feist-Burkhardt, S., Ruckwied, K., 2008. Palynofacies and sea-level changes in the Upper Cretaceous of the Vocontian Basin, Southeast France. Cretaceous Res. 29, 1047–1057.

Gradstein, F.M., Ogg, J.G., Smith, A.G., Agterberg, F.P., Bleeker, W., Cooper, R.A., Davydov, V., Gibbard, P., Hinnov, L.A., House, M.R., Lourens, L., Luterbacher, H-P., McArthur J., Melchin, M.J., Robb, L.J., Sadler, P.M., Shergold, J., Villeneuve, M., Wardlaw, B.R., Ali, J., Brinkhuis, H., Hilgen, F.J., Hooker, J., Howarth, R.J., Knoll, A.H., Laskar, J., Monechi, S., Powell, J., Plumb, K.A., Raffi, I., Röhl, U., Sanfilippo, A., Schmitz, B., Shackleton, N.J., Shields, G.A., Strauss, H., Van Dam J., Veizer J., Van Kolfschoten, Th., Wilson D., 2004. Geological Time Scale 2004. Cambridge University Press, 589 pp.

Gradstein, F.M., Ogg, J.G., Schmitz, M., Ogg G., 2012. The Geologic Time Scale 2012, Elsevier, 2012, 1176 pp.

Haas, J., Götz, A.E., Pálfy, J., 2010. New insights on Late Triassic to Early Jurassic palaeogeography and eustatic history of the NW Tethyan realm: implications from sedimentary and organic facies of the Csővár Basin (Hungary). Palaeogeogr. Palaeoclimatol. Palaeoecol. 291, 456–468.

Hardenbol, J., Thierry, J., Farley, M.B., Jacquin, T., De Graciansky, P.-C., Vail, P.R., 1998. Charts, in: De Graciansky, P.-C., Hardenbol, J., Jacquin, T., Vail, P.R. (Eds.), Mesozoic and Cenozoic Sequence Stratigraphy of European Basins, Soc. Sed. Geol. Spec. Publ., 60.

Holtzapffel, T., 1985. Les minéraux argileux. Préparation. Analyse diffractométrique et détermination. Soc. Géol. Nord, Publi. 12, 136 pp.

Hug, W., 2003. Sequenzielle Faziesentwicklung der Karbonatplattform des Schweizer Jura im Späten Oxford und frühesten Kimmeridge. GeoFocus 7, Fribourg, 155pp.

de Kaenel, E., and Bergen, J.A., 1996. Mesozoic calcareous nannofossil biostratigraphy from Sites 897, 899, and 901, Iberia Abyssal Plain: new biostratigraphic evidence, in: Whitmarsh, R.B., Sawyer, D.S., Klaus, A., and Masson, D.G. (Eds.), Proc. ODP, Sci. Results, 149: College Station, TX (Ocean Drilling Program), 27–59.

de Kaenel, E., Bergen, J.A., Perch-Nielsen, K. von Salis, 1996. Jurassic calcareous nannofossil biostratigraphy of western Europe. Compilation of recent studies and calibration of bioevents. Bull. Soc. géol. Fr. 167, 15–28.

Lees, J.A., Bown, P.R., Young, J.R., Riding, J.B., 2004. Evidence for annual records of phytoplankton productivity in the Kimmeridge Clay Formation coccolith stone bands (Upper Jurassic, Dorset, UK). Mar. Micropaleontol. 52, 29–49.

Lees, J.A., Bown, P.R., Mattioli, E., 2005. Problems with proxies? Cautionary tales of calcareous paleoenvironmental indicators. Micropaleontology 51, 333–343.

Lees, J.A., Bown, P.R., Young, J.R., 2006. Photic zone palaeoenvironments of the Kimmeridge Clay Formation (Upper Jurassic, UK) suggested by calcareous nannoplankton palaeoecology. Palaeogeogr. Palaeoclimatol. Palaeoecol. 235, 110–134.

Martin-Chivelet, J., Berástegui, X., Rosales, I., Vilas, L., Vera, J.A., Caus, E., Grafe, K.-U. Mas, R., Puig, C., Segura, M., Robles, S., Floquet, M., Quesada, S., Ruiz-Ortiz, P.A., Fregenal-Martınez, M.A., Salas, R., Arias, C., Garcı´a, A., Martin-Algarra, A., Meléndez, M.N., Chacon, B., Molina, J.M., Sanz, J.L., Castro, J.M., Garcia-Hernandez, M., Carenas, B., Garcia-Hidalgo, J., Gil, J., Ortega, F., 2002. Cretaceous. In: Gibbons, W., Moreno, M.T. (Eds.), The Geology of Spain. Geological Society, London, pp. 255–292.

Martin-Garin, B., Lathuilière, B., Geister, J., 2012. The shifting biogeography of reef corals during the Oxfordian (Late Jurassic). A climatic control? Palaeogeogr. Palaeoclimatol. Palaeoecol. 365-366, 136–153.

Mattioli, E., 2006. Le nannoplancton calcaire durant l'événement anoxique du Toarcien inférieur : implications pour la paléocéanographie de la Téthys occidentale. Unpublished Mémoire d'habilitation à diriger des recherches, Université Claude Bernard Lyon 1, 90 pp.

Mattioli, E., Pittet, B., 2004. Spatial and temporal distribution of calcareous nannofossils along a proximal-distal transect in the Umbria-Marche basin (Lower Jurassic; Italy). Palaeogeogr. Palaeoclimatol. Palaeoecol. 205, 295–316.

Matyja, B.A., Wierzbowski, A., Wright, J.K., 2006. The Sub-Boreal/Boreal ammonite succession at the Oxfordian/Kimmeridgian boundary at Flodigarry, Staffin Bay (Isle of Skye), Scotland. Transactions of the Royal Society of Edinburgh: Earth Sciences 96, 387–405.

Moore, D.M., Reynolds, R.C., 1989. X-ray diffraction and the identification and analysis of clay minerals. Oxford Univ. Press, New York, 332 pp.

Mutterlose, J., 1991. Das Verteilungs- und Migrationsmuter des kalkigen ? Nannoplanktons in der borealen Unterkreide (Valangin-Apt). Palaeontographica B, 221, 27–152.

Ogg, J.G., Ogg, G., Gradstein, F.M., 2008. The Concise Geologic Time scale. Cambridge University Press, 150 pp.

Osete, M.L., Gómez, J.J., Pavón-Carrasco, F.J., Villalaín, J.J., Palencia-Ortas, A., Ruiz-Martínez, V.C., Heller, F., 2011. The evolution of Iberia during the Jurassic from palaeomagnetic data. Tectonophysics 502, 105–120.

Pellenard, P., Deconinck, J.-F., 2006. Mineralogical variability of Callovo-Oxfordian clays from the Paris Basin and the Subalpine Basin. C.R. Geoscience, 338, 854–866.

Pellenard, P., Tramoy, R., Pucéat, E., Huret, E., Martinez, M., Bruneau, L., Thierry, J., 2014. Carbon cycle and sea-water palaeotemperature evolution at the Middle-Late Jurassic transition, eastern Paris Basin (France). Mar. Petrol. Geol. 53, 30–43.

Pettijohn, F.J., Potter, P.E., Siever, R., 1987. Sand and sandstones, second ed. Springer-Verlag, New York, Berlin, Heidelberg, London, Paris, Tokyo.

Pittet, B., Gorin, G.E., 1997. Distribution of sedimentary organic matter in a mixed carbonate-siliciclastic platform environment: Oxfordian of the Swiss Jura Mountains. Sedimentology 44, 915–937.

Pittet, B., Strasser, A., Mattioli, E., 2000. Depositional sequences in deep-shelf environments: a response to sea-level changes and shallow platform carbonate productivity (Oxfordian, Germany and Spain). J. Sediment. Res., 70, 392–407.

Pittet, B., Mattioli, E., 2002. The carbonate signal and calcareous nannofossil distribution (Balingen-Tieringen section, Late Oxfordian, south Germany). Palaeogeogr. Palaeoclimatol. Palaeoecol. 179, 73–98.

Premoli Silvá, I., Erba, E., Tornaghi, M., 1989. Paleoenvironmental signals and changes in surface fertility in Mid Cretaceous Corg-Rich pelagic facies of the Fucoid Marls (Central Italy). Geobios 22, 225–236.

Roth, P.H., 1981. Mid-Cretaceous calcareous nannoplankton from the Central Pacific: implications for paleoceanography, in: Thiede, J., et al. (Ed.), Initial Reports of the Deep Sea Drilling Project 62, 471–489.

Roth, P.H., 1983. Jurassic and Lower Cretaceous calcareous nannofossils in the western North Atlantic (Site 534): biostratigraphy, preservation, and some observations on biogeography and paleoceanography, in: Sheridan, R.E., Gradstein, F.M., et al. (Eds.), Initial Reports of the Deep Sea Drilling Project 76, 587–621.

Roth, P.H., Bowdler, J., 1981. Middle Cretaceous nannoplankton biogeography and oceanography of the Atlantic Ocean, in: Warme, J.E., Douglas, R.G., Winterer, E.L., (Eds.), The Deep Sea Drilling Project: a Decade of Progress. S. E. P. M. Spec. Publ. 32, 517–546.

Roth, P.H., Krumbach, K.R., 1986. Middle Cretaceous calcareous nannofossil biogeography and preservation in the Atlantic and Indian oceans: implications for paleoceanography. Mar. Micropaleontology 10, 235–266.

Salas, R., Casas, A., 1993. Mesozoic extensional tectonics, stratigraphy and crustal evolution during the Alpine cycle of the eastern Iberian basin. Tectonophysics 228, 33–55.

Saint-Germès, M., Baudin, F., Deconinck, J.-F., Hantzpergue, P., Samson, Y., 1996. Sédimentologie de la matière organique et des argiles du Kimméridgien de Normandie (région du Havre). Géologie de la France 3, 21–33.

Schnyder, J., Baudin, F., Deconinck, J.-F., Durlet, C., Jan Du Chêne, R., Lathuilière, B., 2000. Stratigraphie et analyse sédimentologique du passage Oxfordien-Kimméridgien dans le Boulonnais. Géologie de la France, 4, 21–37.

Steffen, D., Gorin, G.E., 1993. Palynofacies of the Upper Tithonian-Berriasian deep-sea carbonates in the Vocontian Trough (SE France). B. Cent. Rech. Expl.-Prod. Elf-Aquitaine 17, 235–247.

Strasser, A., Pittet, B., Hillgärtner, H., Pasquier, J.-B., 1999. Depositional sequences in shallow carbonate-dominated sedimentary systems: concepts for a high-resolution analysis. Sediment. Geol. 128, 201–221.

Strasser, A., Aurell, M., Bádenas, B., Meléndez, G., Tomás, S., 2005. From platform to basin to swell: orbital control on sedimentary sequences in the Oxfordian, Spain. Terra Nova 17, 407–413.

Summerhayes, C.P., 1987. Organic-rich Cretaceous sediments from the North Atlantic, in: Brooks, J., Fleet, A.J. (Eds.), Marine petroleum source rocks, Geol. Soc. Lon., Spec. Public. 26, 301–316.

Tyson, R.V., 1993. Palynofacies analysis, in: Jenkins, D.G. (Ed.), Applied Micropaleontology, Kluwer Academic Publishers, Dordrecht, pp. 153–191.

Tyson, R.V., 1995. Sedimentary Organic Matter: Organic Facies and Palynofacies. Chapman & Hall, London.

Tyson, R.V., Follows, B., 2000. Palynofacies prediction of distance from sediment source: A case study from the Upper Cretaceous of the Pyrenees. Geology 28, 569–571.

Van Wees, J.D., Arche, A., Beijdorff, C.G., Lopez-Gomez, J., Cloetingh, S., 1998. Temporal and spatial variations in tectonic subsidence in the Iberian Basin (eastern Spain): Interferences from automated modeling of high-resolution stratigraphy (Permian-Mesozoic). Tectonophysics 300, 285–310.

Williams, J. R., Bralower, T. J. 1995. Nannofossil assemblages, fine fraction isotopes, and the paleoceanography of the Valanginian-Barremian (Early Cretaceous) North sea Basin. Paleoceanography 10, 815–839.

Appendix A. Supplementary data

Calcareous nannofossils dataset.

sample numbers	depth (m)	preservation	number of specimens	weigth (g)	volume (ml)	heigth of water (cm)
Rb 3	0.7	E2-O2	301	0.0154	475	2.1
Rb 7	2.5	E2-O2	301	0.0153	475	2.1
Rb 11	3.9	E3-02	301	0.015	475	2.1
Rb 16	5.5	E2-O2	304	0.015	475	2.1
Rb 20	7.7	E3-02	301	0.0151	475	2.1
Rb 22'	8.9	E3-02	300	0.0153	475	2.1
Rb 24	9.68	E3-02	302	0.015	475	2.1
Rb 26	10.3	E3-02	304	0.015	475	2.1
Rb 29	13.1	E3-O2	301	0.0153	475	2.1
Rb 30'	14.4	E2-O2	150	0.0151	475	2.1
Rb 38	34.1	E3-O2	254	0.0185	475	2.1
Rb 42	36.2	E3-O2	159	0.0165	475	2.1
Rb 46	38.9	E2-O2	193	0.015	475	2.1
Rb 52	43.45	E3-O2	290	0.015	475	2.1
Rb 56	49.05	E3-O2	302	0.015	475	2.1
Rb 62	51.9	E3-O2	151	0.015	475	2.1
Rb 65	54.72	E2-O2	233	0.015	475	2.1
Rb 68	56.1	E3-O2	150	0.0186	475	2.1
Rb 70	57.9	E3-O2	151	0.015	475	2.1
Rb 73	60,00	E3-O2	149	0.0161	475	2.1
Rb 77	62.05	E2-O3	185	0.015	475	2.1
Rb 79	63.05	E3-O2	158	0.0157	475	2.1
Rb 81	64.95	E3-O2	151	0.0167	475	2.1
Rb 84	67.85	E3-O2	135	0.0153	475	2.1
Rb 86	68.8	E2-O2	192	0.015	475	2.1
Rb 89	70.9	E3-O3	47	0.0152	475	2.1
Rb 93	73.2	E3-O2	156	0.015	475	2.1
Rb 95	75.6	E3-O2	150	0.015	475	2.1
Rb 98	78,00	E3-O3	42	0.015	475	2.1
Rb 100	79.1	E3-O2	146	0.015	475	2.1
Rb 103	80,00	E3-O2	148	0.015	475	2.1
Rb 105	81.85	E3-O3	51	0.015	475	2.1
Rb 108	83.73	E3-O3	14	0.0152	475	2.1
Rb 111	85.93	E3-O3	18	0.015	475	2.1
Rb 116	89.1	E3-O2	155	0.015	475	2.1
Rb 118	92.3	E3-O2	57	0.0153	475	2.1
Rb 122	95.85	E2-O2	150	0.0152	475	2.1

surface of field of view (cm²)	number of fields of view	sedimentation rate (m/Myr)	Axopodorhabdus cylindratus
0.000201	153		0
0.000201	172		0
0.000201	70	0.000025	1
0.000201	181	0.000025	0
0.000201	337	0.00004	0
0.000201	143	0.00004	0
0.000201	137	0.00004	0
0.000201	311	0.00018	0
0.000201	349	0.00018	1
0.000201	403	0.00018	0
0.000484	228	0.00011	0
0.000484	327	0.00011	0
0.000484	353	0.00011	0
0.000201	389	0.00006	0
0.000201	555	0.000085	0
0.000201	327	0.000085	0
0.000484	371	0.000175	0
0.000201	395	0.000175	0
0.000201	401	0.000175	0
0.000201	327	0.000175	0
0.000484	541	0.000175	0
0.000201	300	0.000175	0
0.000484	509	0.000175	0
0.000484	448	0.000175	1
0.000484	551	0.000175	0
0.000484	289	0.000175	0
0.000484	664	0.0001	0
0.000201	486	0.0001	0
0.000484	411	0.0001	0
0.000484	555	0.0001	0
0.000484	684	0.0001	0
0.000484	470	0.0002	0
0.000484	207	0.0002	0
0.000484	200	0.0002	0
0.000484	556	0.0002	0
0.000484	412	0.0002	0
0.000484	521	0.0002	0

Ansulasphaera helvetica	Biscutum dorsetensis	B. dubium	Bussonius	Crepidolithus crassus	C. perforatus
0	0	0	0	0	0
0	0	0	0	0	0
0	0	0	0	0	0
0	0	0	0	0	0
0	0	0	0	0	0
0	0	0	0	0	0
0	0	0	0	0	0
0	0	0	0	0	0
0	0	0	0	0	0
0	0	0	0	0	0
1	1	0	0	0	1
0	0	0	0	0	0
0	1	0	0	0	0
0	0	0	0	0	0
0	0	0	0	0	0
0	0	0	0	0	0
0	1	0	0	0	0
0	0	0	0	0	0
0	0	0	0	0	0
0	0	0	0	0	0
0	0	1	0	0	0
0	1	0	0	0	0
0	1	0	1	0	0
0	0	0	0	1	0
1	0	0	0	0	0
0	0	0	0	0	0
0	0	0	0	0	0
0	0	0	0	0	0
0	0	0	0	0	0
0	0	0	0	0	0
0	0	0	0	0	0
0	1	1	0	0	0
0	0	0	0	0	0
0	0	0	0	0	0
0	0	0	0	0	0
0	0	0	0	0	0
0	0	0	0	0	0
1	0	0	0	0	0

Cyclagelosphaera margerelii	C. wiedmannii	Diazomatolithus lehmanii	Discorhabdus criotus	D. ignotus
19	1	0	0	0
27	0	0	0	0
22	1	1	0	1
27	0	0	0	0
28	0	0	1	0
28	0	0	0	0
25	0	1	1	0
48	0	1	0	0
50	0	0	0	0
23	0	0	0	0
16	0	0	1	0
14	0	0	1	0
23	0	0	1	0
23	0	0	0	0
39	0	0	4	0
14	0	0	0	0
30	0	0	0	1
14	0	0	0	0
12	0	0	0	0
17	0	0	0	0
26	0	0	0	0
22	0	0	0	0
23	1	0	0	0
11	0	0	0	0
22	0	0	0	2
2	0	0	0	0
29	0	0	0	0
16	0	0	1	0
7	0	0	0	0
25	0	0	0	0
28	0	0	0	0
16	0	0	0	0
5	0	0	0	0
2	0	0	0	0
29	0	0	0	0
10	0	0	0	1
44	0	0	0	2

D. striatus	Discorhabdus indet.	Ethmorhabdus gallicus	Hexalithus	Lotharingius barozii	L. crucicentralis
0	0	1	0	0	0
0	0	0	0	0	0
0	0	1	0	0	1
0	0	0	0	0	0
0	0	0	0	0	0
0	0	2	0	0	0
0	0	0	0	0	0
0	0	0	0	0	0
0	0	1	0	0	0
0	0	0	0	0	0
0	0	0	0	0	0
0	0	0	2	0	0
0	0	1	0	0	0
0	0	0	0	0	0
0	0	0	0	0	0
0	0	0	0	0	0
2	1	0	0	0	0
0	0	0	0	0	0
0	0	0	0	0	0
0	0	0	0	0	0
0	0	0	0	0	0
0	0	0	0	0	0
0	0	0	0	0	0
0	0	0	1	0	1
0	0	0	1	0	0
0	0	0	0	0	0
0	0	0	0	1	0
0	0	0	0	0	0
0	0	0	0	0	0
0	0	0	0	0	0
0	0	0	0	0	0
0	0	0	0	0	0
0	0	0	0	0	0
0	0	0	0	0	0
0	0	0	0	0	0
0	1	0	1	0	0

L. frodoi	L. hauffii	L. velatus	Lotharingius indet.	Mazaganella protenza	Miravetesina favula
0	4	0	2	0	0
1	10	2	2	0	0
4	18	0	3	0	0
1	26	2	2	0	0
1	31	1	7	0	0
1	35	1	2	0	0
2	30	1	0	0	0
3	29	2	5	0	0
5	18	0	3	0	0
0	2	0	3	0	0
10	25	11	16	0	0
4	5	2	0	0	1
6	7	2	6	0	2
0	38	0	0	0	0
0	11	5	18	0	0
0	7	0	0	1	0
1	5	0	2	0	0
1	19	0	5	0	0
0	15	3	5	0	0
0	0	0	0	0	0
8	4	2	1	0	0
0	6	0	2	0	0
9	7	4	7	0	2
6	3	1	3	0	2
8	11	4	4	0	3
0	1	0	0	0	0
8	4	1	2	0	0
0	11	0	0	0	0
1	3	0	1	0	0
2	4	0	0	0	0
5	2	0	1	0	2
2	1	0	0	0	0
0	1	1	0	0	0
0	0	0	1	0	0
3	2	0	0	0	0
0	1	1	1	0	0
1	0	0	0	0	0

Parhabdolithus liasicus	Polypodorhabdus escaigii	Retecapsa octofenestrata	Rhagodiscus
0	0	0	0
0	0	0	0
0	0	0	0
0	0	0	0
0	0	0	0
0	0	0	0
0	0	0	0
0	0	0	0
0	0	0	0
0	0	0	0
0	0	0	0
0	0	0	0
0	0	0	1
0	0	0	0
0	0	0	0
0	0	0	0
0	0	0	0
0	0	0	0
0	0	0	0
0	0	0	0
1	0	0	0
0	0	1	0
0	2	1	0
0	0	0	0
0	1	0	0
0	0	0	0
0	0	0	0
0	0	0	0
0	1	0	0
0	0	0	0
0	0	0	0
0	0	0	0
0	0	0	0
0	0	0	0
0	1	1	0

Schizosphaerella punctulata	Similiscutum novum	Staurolithites	Stephanolithion bigoti bigoti	S. bigoti maximum
0	0	0	0	0
0	0	0	0	0
2	0	0	0	1
0	0	0	0	1
0	0	0	0	0
0	0	0	0	0
0	0	0	0	0
0	1	0	0	1
0	0	0	0	0
0	0	0	0	0
1	0	0	0	0
1	0	1	1	0
0	0	1	0	0
0	0	0	0	0
0	2	0	0	0
0	1	0	0	0
0	1	1	0	0
0	0	0	0	0
0	0	0	0	0
0	0	0	0	0
0	0	0	0	0
0	0	0	0	0
0	0	1	0	0
0	0	0	0	0
0	1	0	0	0
0	0	0	0	0
0	0	0	0	0
0	0	0	0	0
0	0	0	0	0
0	0	0	0	0
0	0	0	0	0
0	0	0	0	0
0	0	0	0	0
0	0	0	0	0
0	0	0	0	0
0	0	0	0	0
0	0	0	0	0

Triscutum tiziense	Tuborhabdus patulus	Watznaueria barnesiae	W. aff. barnesiae	W. biporta	W. britannica A
0	48	25	5	41	29
0	19	10	2	78	49
0	26	35	5	16	26
0	39	20	3	79	19
0	29	22	0	56	22
0	36	10	0	65	27
0	38	14	4	82	26
0	45	15	3	63	14
0	55	10	4	56	26
0	38	5	2	31	10
0	48	43	4	32	11
0	24	22	0	34	11
0	28	19	1	38	11
0	78	3	1	43	21
0	43	11	6	46	18
0	10	8	2	54	18
0	36	29	0	57	11
0	24	4	1	47	13
0	20	0	0	52	16
0	5	5	7	46	22
0	10	13	0	61	15
0	6	24	6	34	21
2	15	15	3	32	5
2	31	15	0	26	3
0	22	33	0	30	6
0	4	17	1	8	1
0	22	33	0	13	4
0	21	9	5	18	7
0	9	7	0	5	3
0	16	35	0	17	7
0	14	28	0	23	9
0	1	12	0	9	0
0	3	0	0	2	1
0	1	6	0	4	1
0	11	40	0	36	8
0	0	4	5	0	14
0	1	5	24	0	38

W. britannica B	W. britannica C	W. britannica D	W. britannica E	W. britannica F	W. britannica G	W. britannica indet.
0	0	7	1	1	4	9
0	1	13	2	3	16	3
0	4	18	8	10	26	12
0	3	12	9	1	0	3
1	7	6	8	2	14	0
0	5	15	8	1	0	1
0	6	9	9	1	5	3
0	5	12	5	0	0	3
0	5	10	7	2	9	0
0	0	2	0	0	6	0
0	1	0	12	0	3	1
0	1	0	4	0	3	0
0	3	4	8	0	0	1
0	1	14	1	4	23	0
0	5	11	6	6	0	11
1	6	7	6	1	0	6
1	3	9	4	0	0	2
0	2	4	6	0	0	0
0	0	7	7	0	7	0
0	2	12	9	0	0	8
1	3	6	4	0	1	0
0	2	7	3	0	0	1
0	0	2	4	0	1	1
1	0	1	3	0	0	0
2	1	1	12	0	2	0
1	0	1	2	0	0	0
1	10	6	4	0	1	0
0	3	8	6	0	3	3
0	1	1	2	0	0	0
1	4	6	10	0	0	0
1	0	1	3	0	0	0
1	1	1	1	0	0	0
0	0	0	0	0	0	0
0	1	0	0	0	0	0
1	3	0	4	0	0	0
6	0	0	2	1	0	0
15	0	2	0	0	0	0

W. communis	W .contracta	W. fossacincta	W. manivitiae	W. aff. manivitiae	W. manivitiae/britannica
0	10	48	32	5	9
0	7	12	21	3	20
0	0	23	29	0	7
0	10	14	19	3	11
0	11	11	34	2	7
0	5	17	18	2	19
0	6	16	7	2	13
0	7	3	12	0	25
0	8	3	9	2	17
0	4	3	12	0	9
2	1	2	1	0	7
2	0	0	5	0	14
0	2	4	3	2	18
0	0	0	7	3	30
0	1	3	8	5	36
0	4	1	3	0	0
1	0	1	8	2	22
0	0	0	2	0	6
0	1	0	0	0	5
0	0	0	9	1	6
0	1	3	4	2	19
0	5	3	0	1	13
0	0	2	1	1	10
0	0	0	1	0	21
0	2	3	5	1	10
0	0	3	0	2	4
1	1	1	2	1	8
0	0	5	19	9	6
0	0	0	0	0	1
0	0	2	4	4	9
0	0	5	12	3	9
0	0	0	1	1	2
0	1	0	0	0	0
0	0	0	1	1	0
0	0	0	7	3	8
0	0	0	0	1	0
0	0	0	1	3	3

Watznaueria indet.	Zeugrhabdotus erectus	sp. 1	non identified specimens
0	0	0	
0	0	0	
0	0	0	
0	0	0	
0	0	0	
2	0	0	
0	0	1	
0	0	2	
0	0	0	
0	0	0	
0	1	3	
0	1	6	
0	0	0	
0	0	0	
0	0	6	
0	0	2	
0	1	1	
0	0	2	
1	0	0	
0	0	0	
0	0	0	
0	0	1	
0	1	0	
0	0	0	
0	0	2	
0	0	0	
2	0	0	
0	0	0	
0	0	0	
0	0	0	
1	0	0	
0	0	0	
0	0	0	
0	0	0	
0	0	0	
10	0	0	0
5	0	1	0